S29434, a Quinone Reductase 2 Inhibitor: Main Biochemical and Cellular Characterization

Jean A. Boutin, Frédéric Bouillaud, Elzbieta Janda, István Gacsalyi, Gerald Guillaumet, Etienne C. Hirsch, Daniel A Kane, Françoise Nepveu, Karine Reybier, Philippe Dupuis, et al.

S29434, a quinone reductase 2 reference inhibitor: main biochemical and cellular characterization.

Jean A. Boutin[1],*,**, Frederic Bouillaud[2], Elzbieta Janda[3], István Gacsalyi[4],***, Gérald Guillaumet[5], Etienne C. Hirsch[6], Daniel A. Kane[7], Françoise Nepveu[8], Karine Reybier[8], Philippe Dupuis[9], Marc Bertrand[10], Monivan Chhour[8], Thierry Le Diguarher[10], Mathias Antoine[1], Karen Brebner[7], Hervé Da Costa[5,11], Pierre Ducrot[1], Adeline Giganti[1], Vishalgiri Goswami[12], Hala Guedouari[2], Patrick P. Michel[6], Aakash Patel[12], Jérôme Paysant[13], Johann Stojko[1], Marie-Claude Viaud-Massuard[11], Gilles Ferry[1]

[1] Pôle d'Expertise Biotechnologie, Chimie & Biologie, Institut de Recherches SERVIER, 78290 Croissy-sur-Seine, France

[2] Institut Cochin, INSERM U1016, CNRS-UMR8104, Université Paris Descartes 75014 Paris, France

[3] Department of Health Sciences, Magna Graecia University, 88100 Catanzaro, Italy

[4] Egis Pharmaceuticals PLC, 1165 Budapest, Hungary.

[5] Institut de Chimie Organique et Analytique (ICOA), Université d'Orléans, UMR CNRS 7311, 45067 Orléans Cedex 2, France

[6] Institut du Cerveau et de la Moelle épinière, ICM, Inserm U 1127, CNRS UMR 7225, Sorbonne Université, F-75013, Paris, France

[7] Departments of Human Kinetics (DK) and Psychology (KB), St. Francis Xavier University, Antigonish, NS, Canada

[8] UMR 152 Pharma-Dev, Université de Toulouse, IRD, UPS, 31062 Toulouse, France

[9] EUROFINS-CEREP SA, 86600 Celle L'Evescault, France

[10] Technologie Servier, Orléans, France

[11] CNRS-UMR 7292 « GICC Innovation Moléculaire et Thérapeutique », Université de Tours, 37200 Tours, France

[12] Oxygen Healthcare Pvt Ltd, 382213 Ahmedabad, Gujarat, India

[13] Pôle d'Innovation Thérapeutique de Cardiologie, Institut de Recherches SERVIER, 92150, Suresnes, France

* : Corresponding author : jean.boutin@servier.com Institut de Recherches Internationales SERVIER, 50 rue Carnot, 92150 Suresnes, France Tel +33(0)155724400

**: present address Institut de Recherches Internationales Servier, 92150 – Suresnes

*** : present address : ATRC Aurigon Ltd., Budapest, Hungary

Running title: Reference quinone reductase 2 inhibitor: S29434.

Abbreviations: BNAH: *N*-benzyldihydronicotinamide; CLQ: chloroquine; DIPEA: *N*,*N*-diisopropylethylamine; DMEM: Dulbecco's modified essential medium ; DMF: dimethylformamide; FBS: fetal bovine serum; HATU: hexafluorophosphate azabenzotriazole tetramethyl uronium or 1-[bis(dimethylamino)methylene]-1*H*-1,2,3-triazolo[4,5-b]pyridinium 3-oxid hexafluorophosphate; ITC: isothermal titration calorimetry; MPP+: 1-methyl-4-phenylpyridinium; MPTP: 1-methyl-4-phényl-1,2,3,6-tetrahydropyridine; NaH: sodium hydride; NRH: *N*-ribosyldihydronicotinamide; QR1: NAD(P)H dehydrogenase (quinone 1), EC 1.6.5.2; QR2: quinone reductase 2 or ribosyldihydronicotinamide dehydrogenase (quinone), formerly E.C. 1.10.99.2 now E.C. 1.10.5.1 ; ROS: reactive oxygen species; S29434: [2-(2-methoxy-5*H*-1,4b,9-triaza(indeno[2,1-a]inden-10-yl)ethyl]-2-furamide; TCEP: tris(2-carboxyethyl)phosphine; TES: 2-[tris(hydroxymethyl)-methylamino]-ethanesulfonic acid; THF: tetrahydrofuran.

- The number of text pages: 40,
- Number of tables: 1,
- Number of figures: 13,
- Number of references: 80
- Words in Abstract: 177,
- Words in Introduction: 738
- Words in Discussion: 1897

Abstract: Quinone reductase 2 (QR2, E.C. 1.10.5.1) is an enzyme with a feature that has attracted attention for several decades: in standard conditions, it does not recognize NAD(P)H as an electron donor but instead recognizes some putative metabolites of NADH such as *N*-methyl- or *N*-ribosyl-dihydronicotinamide. Several publications have showed in recent years its implication in various systems, particularly related to reactive oxygen species (ROS) on one hand and memory on another, thus strongly suggesting a link between Quinone reductase 2 (as a possible key element in pro-oxidation), autophagy and neurodegeneration in various pathological conditions. In molecular and cellular pharmacology, a lack of specific and powerful tools often is an obstacle to understanding physiopathological associations. Here we present a thorough description of the potent, nanomolar inhibitor S29434 from chemical, molecular, cellular and stability perspectives, including its actions (and lack thereof) in various ROS-producing systems. The inhibitor is fairly stable *in vivo*, penetrates cells, specifically inhibits quinone reductase 2, and has various activities that suggest a key role for this enzyme in different types of pathological conditions including neurodegenerative diseases.

Introduction

Quinone reductases are pyridine nucleotide–dependent enzymes involved in the detoxification of natural quinones, described as early as 1954 in peas (Wosilait and Nason, 1954). In mammals, the reference quinone reductase enzyme, initially designated DT-diaphorase, was first described by Conover and Ernster (1960). In the 1990s, another quinone reductase was cloned: quinone reductase 2 (QR2 or NQO2) with an unusual history (Zhao et al., 1997). Indeed, the initial description pointed at this enzyme to be a strict analogue of quinone reductase 1 (a.k.a., DT-diaphorase, or NAD(P)H dehydrogenase (quinone 1), QR1, NQO1, E.C. 1.6.5.2) with similar properties, but later research revealed that it was quite different from its closest relative. Early research in the 1960s identified QR2 as the only reductase using non-canonical co-substrates such as *N*-ribosyl- and *N*-methyl-dihydronicotinamide and para-quinones as substrates (Liao and Williams-Ashman, 1961; Liao et al., 1962), but not NADH or NADPH (Zhao et al., 1997; Ferry et al., 2010). Later, Talalay and colleagues cloned and crystallized QR2 (Zhao et al., 1997). However, the physiologic role of the enzyme and its specificity were poorly documented and understood, except for the fact that QR2 could recognize non-quinone compounds such as CB1954 as a substrate (Wu et al., 1997). This finding was the basis for attempts to develop CB1954 as a prodrug with interesting cytotoxic properties (Knox et al., 2003). QR2 has been implicated in various situations, distantly related to quinone metabolism, such as antimalarial actions (Kwiek et al., 2004; Cassagnes et al., 2017), AMPA-signaling pathway (Rappaport et al., 2015), paraquat-mediated toxicity (Janda et al., 2013), oxidative stress sensing (Leung and Shilton, 2013) and oocytes maturation (Chen et al., 2017)

While searching for the elusive melatonin MT3 binding site, described by Dubocovich and colleagues (Duncan et al., 1988) and our team (Paul et al., 1999), we found that this binding site was QR2 (Nosjean et al., 2000). A screen of many compounds from our library

[comprising natural products such as flavonoids (Boutin et al., 2005)] added further compounds to the list of QR2 inhibitors, together with the already described resveratrol (Buryanovskyy et al., 2004), tacrine (den Braver-Sewradj et al., 2017) or chloroquine (CLQ) (Kwiek et al., 2004), dabigatran, a prescribed thrombin inhibitor (Michaelis et al., 2012) and tetracyclic compounds (Boussard et al., 2006) such as S29434. Since some of the products of the reduction of quinones are fairly unstable, especially in the absence of conjugating system(s), the products of the reaction, quinols, may spontaneously yield back the original quinones in the presence of oxygen. Similar quinone cycling was described for QR1 (Bindoli et al., 1990; Nutter et al., 1992; Bian et al., 2017). Of note, in the absence of cellular conjugating capacities that neutralize the process by conjugating the quinol (*e.g.* menadiol) with glucuronic acid (Kappus and Sies, 1981; Bolton et al., 2000; Nishiyama et al., 2010), the by-product of this futile cycle is the production of reactive oxygen species (ROS). The generation of ROS can be detected by electron paramagnetic resonance spectroscopy (EPR) (Reybier et al., 2011). Thus, we used that way to show that under some conditions, the pro-oxidant property of QR2 can be confirmed and measured.

QR2 is expressed in many different organs and cells (Nosjean et al., 2001) and might have a key role in several pathological conditions. This makes QR2 an interesting study case. For this reason, we sought to generate new data on the specificity of S29434, its actions in several situations and put them in perspective with the already available data on this inhibitor to consolidate its use as an established QR2 inhibitor tool. The present paper deals with the full description of the characteristics of the inhibitor S29434. Despite previous uses in several publications, no report exists on its synthesis, on the specificity toward alternative enzymes or receptors, or on its characteristics in term of metabolism. Thus, we brought as much information as possible on this molecule, in order to make its use ‘safer’ in term of pharmacology of QR2. Here we cover the most important characteristics of the compound,

from chemistry to molecular and cellular pharmacology, hints of its specificity towards other ROS-generating systems as well as some activities *in vivo*. These data illustrate that S29434 or one of its unknown metabolite(s) reaches QR2 and inhibits this enzyme in situ. Furthermore, its specificity seems to be limited to QR2, making this compound a valuable tool for understanding the role of this enzyme in multiple scenarios, even in vivo.

Materials and Methods

Chemical syntheses. S29434 synthesis has never been published. Two different paths were explored for its synthesis. Both are summarized in **Fig. 1 & 2**. The synthetic routes are given in full details in the supplementary materials, as well as the various steps permitting to obtain the compounds are detailed in the **Supplementary data 1**. The final analyses of the product obtained with the second route are available as **Supplemental Data 1** (spectral analyses of compounds 3, 4 and S29434 obtained by the first synthetic route). S29434 was obtained with purity above 99%. Analytical details of the second route **Supplementary Figure S2** is also given as **Supplementary Data 2, 3, 4, 5, 6 and 7.**

QR2 inhibition measurements. The potency of S29434 was measured in standard kinetic assays. Briefly, QR2 enzymatic activity was measured under FAD saturation using substrate (menadione) and 100 µM co-substrate BNAH or NRH. An oxidoreduction reaction was performed at 25 °C in a Tris–HCl 50 mM, pH 8.5, FAD 500 nM, octyl-glucopyranoside 1 mM, dimethylsulfoxide (DMSO) 5% buffer. Enzymatic kinetics measured the decrease in co-substrate absorbance corresponding to its oxidation. This reaction was followed either at 350 nm (BNAH) or 340 nm (NRH) on a FLUOstar 384-well plate reader (BMG, Offenburg, Germany). The slope of absorbance decrease was determined using FLUOstar Optima software (BMG) and expressed in units of optic density (UDO).s-1 then in M.s-1 using the Beer–Lambert law. This measurement was next corrected from its corresponding non-enzymatic (spontaneous) oxidation rate measured in the absence of enzyme, which corresponds to the specific maximum-activity oxidoreduction reaction. For the inhibitory hQR2 enzymatic activity assay, S29434 was used in the range of 50 pM to 5 µM. The inhibitory concentration 50 % (IC_{50}) and the inhibition percentage of co-substrate oxidation were determined using the PRISM program (GraphPad Software Inc., San Diego, CA, USA).

These experiments were conducted over 50 times (inhibition, **Fig. 3A**) or in triplicate (**Fig. 3B**).

Binding kinetics of S29434 and resveratrol to QR2 FADox (oxidized FAD). Transient kinetics were measured at 25 °C (S29434) or 4 °C (resveratrol) with a SFM-300 stopped-flow mixer fitted with a FC-15 cell and coupled to a MOS-200 M rapid spectrophotometer equipped with a 150 W Xe−Hg lamp (Bio-Logic Science Instruments, Seyssinet-Pariset, France). Typical mixing dead time was 2.6 ms. QR2 tryptophans were excited at 295 nm to minimize photobleaching and excitation of tyrosines. Fluorescence emission was recorded using a 320-nm cutoff filter combined with a UG11 band-pass filter to block S29434 fluorescence. Binding experiments were performed under pseudo-first-order conditions by mixing an equal volume (75 µl) of QR2 and ligand in Tris–HCl 50 mM, β-octyl-D-glucopyranoside 1 mM, DMSO 5%, pH 8.5. QR2 monomer concentration after mixing was 1 µM. Fluorescence traces were first analyzed individually with the BioKine software (Bio-Logic, v4.80) as the sum of up to two exponential terms, as described by equation 1, with n being the number of exponentials, ai the amplitude of the ith exponential, kobs i the rate constant of the ith exponential, c the trace end point, and bt accounting for the slow linear drift caused by photobleaching. **Fig. 4** was generated with Prism (GraphPad, v7.03).

$$y = \left(\sum_{i=1}^{n} a_i e^{(-k_{obs\,i}\, t)} \right) + bt + c \qquad (1)$$

The kobs values were plotted against ligand concentration. When a linear increase of kobs was observed, data were fitted to equation 2 describing a one-step binding mechanism, using Prism (GraphPad, v7.03).

$$k_{obs} = k_1[\text{ligand}] + k_{-1} \qquad (2)$$

Specificity tests. *General specificity*. Most of the tests were subcontracted to Eurofins. All experimental details can be found online on their site (www.eurofinsdiscoveryservices.com).

Specificity tests. *Kinases*. The panel of kinases for screening is available from Eurofins (ExpressDiversityKinase). It comprises 46 different kinases chosen to cover a maximal structural diversity among this large family of over 500 different enzymes. S29434 was tested at 100 nM on the acticity of all the kinases using a standard radiometric assay.

Specificity tests *Sirtuin experiments*. The use of this original technology has been reported in a technical note by Agilent (see https://www.agilent.com/cs/library/applications/5990-9345en_lo.pdf). In brief, recombinant sirtuin 1 (SIRT1) was produced in E. coli and purified. The non-acetylated and acetylated Foxo-3 substrates (hFoxo-3a-290-K(Ac): Ac-DSPSQLS-K(Ac)-WPGSPTS-NH2) were synthesized by GENEPEP SA (Saint-Jean-de-Védas, France). Deacetylase reactions were carried out in reaction buffer (Tris–HCl 50 mM, NaCl 137 mM, KCl 2.7 mM, MgCl2 1 mM, bovine serum albumin 0.05%, TCEp 1 mM, NAD+ 0.8 mM) and 20 nM SIRT1 for 30 min at room temperature. The reaction was initiated by the addition of peptide substrate and quenched by the addition of 2% formic acid. The transitions of peptides detection: substrate: (excitation at 829.1 nm; emission at 544.6 nm) and product (excitation at 808.4 nm; emission at 544.5 nm) were detected.

Specificity tests. *NAD(P)H oxidase experiments*. This enzyme activity was measured using the lucigenin assay as described by Sasaki et al. (2013) and by Kuribayashi et al. (2008). This assay was adapted to the U937 cell line as biological source.

ROS production in acellular and cellular experiments using electron paramagnetic resonance (EPR). 5,5'-dimethyl-1-pyrroline *N*-oxide (DMPO) were purchased from Interchim (Montluçon, France). Menadione, adrenochrome, 3,3'-methylene-bis(4-hydroxycoumarin) (dicoumarol), NADH, and PBS were purchased from Sigma-Aldrich-Fluka Co. (Saint Quentin Fallavier, France). BNAH was purchased from TCI Europe (Zwijndrecht,

Belgium). NRH was custom synthesized by O2h (Ahmedabad, India). DMSO was purchased from Fisher (UK, Loughborough). The DMPO stock solution (1 M) was prepared in water and stored at -80 °C until required. The inhibitors (S29434 and dicoumarol) were prepared as 1 mM solutions in DMSO and diluted in PBS to yield 0.2 mM. The substrates and co-substrates stock solutions were prepared in DMSO. Experiments on pure enzyme were performed with demineralized (18 MΩ) and deaerated water containing tris(hydroxymethyl)amino-methane 50 mM and ß-octyl-glucoside 1 mM, final pH 8.5. A Chinese hamster ovary cell line overexpressing QR2 (CHO-k1-QR2) was described previously (Cassagnes et al., 2015). The experiments were performed on 5.10^6 cells suspended in a final volume of 400 µl. EPR spectra were obtained at X-band and at room temperature on a Bruker EMX-8/2.7 (9.86 GHz) equipped with a high-sensitivity cavity (4119/HS 0205) and a gaussmeter (Bruker, Wissembourg, France). The analyses were performed with a flat quartz cell FZKI160-5 X 0.3 mm (Magnettech, Berlin, Germany). WINEPR and SIMFONIA software programs (Bruker) were used for EPR data processing and spectrum computer simulation. Typical scanning parameters were as follows: scan number, 5; modulation amplitude, 1 G; modulation frequency, 100 kHz; microwave power, 1 mW; sweep width, 100 G; sweep time, 41.94 s; time constant, 20.48 ms; and magnetic field 3465–3560 G. The intensities of the EPR signals were evaluated by measuring the amplitude peak to peak of the second line.

Liver and brain mitochondrial respiration. The animal experimentation component of the studies was conducted with the approval of the local Animal Care and Use Committee and according to the applicable guidelines of the CNRS (http://www.cnrs.fr/infoslabos/reglementation/euthanasie2.htm). Rats (male, 150 g) were sacrificed by cervical dislocation followed by decapitation (fast bleeding). The liver and brain were quickly removed and placed in ice-cold mitochondria isolation buffer (sucrose 300

mM, Tris 10 mM, EGTA 1 mM, pH 7.4). Mitochondria were prepared by differential centrifugation, and the final mitochondrial pellet was resuspended in isolation buffer (20–80 mg/mL). Mitochondria were resuspended in 5 mL of mitochondrial respiration buffer (KCl 100 mM, sucrose 40 mM, TES 10 mM, $MgCl_2$ 5 mM, EGTA 1 mM, 5 mM phosphate, fatty acid–free bovine serum albumin 0.4 %, pH 7.2), and this suspension was distributed in each of the two chambers (2 mL final volume) of the Oxygraph 2K (Oroboros Instruments, Innsbrück, Austria). Temperature was set to 25 °C. Respiration was initiated with addition of glutamate and malate (5 mM each), and a fully stimulated phosphorylating state 3 was obtained by addition of 1.25 mM ADP. Increasing amounts of the S29434 were added to one chamber using 1,000 × concentrated working solutions in DMSO, and simultaneously the same volume (2 µl) of DMSO was added in the other chamber.

Muscle mitochondrial respiration. With the exception of Amplex Red Ultra (Life Technologies) and BNAH (see above), all chemicals and reagents were purchased from Sigma-Aldrich. Male Wistar rats were purchased from Charles River Laboratories, Inc. (Montréal, QC) and acclimated for approximately 2 weeks in the Animal Care Facility at St. Francis Xavier University (Canada). During the acclimation period, the rats were housed in pairs in standard cages with a plastic tunnel to provide environmental enrichment. All rats had access to standard rat chow and water, ad libitum. The room in which the rats were housed was maintained at 20 °C/22 °C and 40%/60% relative humidity and on a reversed 12-h light/dark cycle. Approval was granted by the institutional Animal Care Committee at St. Francis Xavier University prior to commencing the study, in accordance with guidelines of the Canadian Council on Animal Care guidelines. Variations of the permeabilized myofiber preparation are published elsewhere (Kuznetsov et al., 2008; Perry et al., 2011; Pesta and Gnaiger, 2012; Perry et al., 2013). In brief, immediately following euthanasia with sodium pentobarbital, two cuts were made on the right gastrocnemius muscle of each animal. Red

(i.e., oxidative) portions of the gastrocnemius were extracted and placed in ice-cold buffer X, consisting of (in mM): 50 MES, 7.23 K_2EGTA, 2.77 CaK_2EGTA, 20 imidazole, 0.5 DTT, 20 taurine, 5.7 ATP, 14.3 phosphocreatine, and 6.56 $MgCl_2.6H_2O$ (pH 7.1). Four fiber bundles from each gastrocnemius section were separated along the longitudinal axis, using needle tipped forceps (Fine Science Tools, Inc., Vancouver, CB, Canada) in ice-cold buffer X under magnification (Discovery V8, Carl Zeiss, Oberkochen, Germany). Following dissection, fiber bundles were placed in vials containing saponin (50 μg/mL) dissolved in 2.0 mL of buffer X. These vials were then placed on a nutating mixer (VWR International, Radnor, PA, USA) and kept at 4 °C for 30 min. After permeabilization, fiber bundles were transferred to a wash buffer solution, MiR05, consisting of (in mM): 20 taurine, 0.5 EGTA, 3 $MgCl_2$, 60 K-lactobionate, 10 KH_2PO_4, 20 HEPES, 110 sucrose, 20 creatine, 1 g/L fatty acid–free bovine serum albumin, pH 7.1. Fiber bundles remained in MiR05 for approximately 15 min with regular inversion on the nutating mixer until experimentation, after which the samples were placed into the Oxygraph-2k (Oroboros). Blebbistatin was included in the permeabilization buffer, wash buffer, and assay to inhibit spontaneous contraction of muscle fibers (Perry et al., 2011; Perry et al., 2013). Substrate-dependent respiratory oxygen consumption was measured with the Oxygraph 2K (Oroboros). H_2O_2 production was monitored in permeabilized rat red gastrocnemius muscle fibers simultaneously with respirometry using an amperometric add-on LED module to the Oroboros Oxygraph-2k. Prior to the first substrate addition of the respirometric protocol, 10 μM Amplex Red Ultra, 5 U/mL superoxide dismutase, and 1 U/mL horseradish peroxidase were added to the oxygraph chambers containing the fibers. H_2O_2 calibration experiments were performed under the same parameters used for experimental data collection. The relationship between H_2O_2 and fluorescence intensity was linear to at least 0.7 μM. Next the following were added, in order: 4 mM malate, 0.2 mM octanoylcarnitine, 5 mM ADP, 20 mM L-lactate, 5 mM NAD+, 5 mM pyruvate, and 10 μM

UK-5099, and 10 mM glutamate was then added to test glutamate oxidation. Then, 10 mM succinate, 1 μM auranofin (thioredoxin reductase inhibitor), and 100 μM carmustine (BCNU; inhibitor of thioredoxin and glutathione reductases) were added to the chambers consecutively to inhibit the H_2O_2 scavenging systems mitochondria. Finally, H_2O_2 was titrated to internally calibrate the resorufin signal for H_2O_2. Following conclusion of the respirometry experiments, fibers were placed directly into water to clear out any remaining substrates in the cytosol. After 5 min, fiber bundles were then placed in a clean dry Eppendorf tube and freeze-dried using Labconco® FreeZone1. Following freeze-drying for 5 h, fiber bundles were weighed on a Mettler Toledo® Excellence Plus XP6 Ultra-Microbalance.

Data are expressed as mean ± SEM. A two-way, repeated measures ANOVA was completed for each oxygen flux and hydrogen peroxide production to identify any interaction among the three groups of exercise and histamine receptor antagonists, exercise only, and control. This step was followed by a one-way ANOVA with repeated measures (Bonferroni post hoc analysis) to examine differences between different substrate additions. Data analysis was completed using Prism 7 (GraphPad). The α-level for statistical significance was set at 0.05.

Measurement of mitochondrial ROS levels by flow cytometry in cells. MitoSox (Thermo Fisher ScientificLife Tech., Molecular probes, Waltham, MA, USA) was used to measure mitochondrial superoxide levels in cells by flow cytometry. HepG2 were a kind gift from Dr. Eugenio Arcidiacono (University Magna Graecia, Catanzaro, Italy), were cultured in high-glucose (4.5 g/L) Dulbecco's modified essential medium (DMEM), as described (Lascala et al., 2018). U373 cells were cultures in low-glucose DMEM. Both types of DMEM were supplemented with 10 % fetal bovine serum (FBS), 1 % penicillin and streptomycin solution (Pen-Strep) and 1 % glutamine, all from Carlo Erba srl (Milan, Italy). HepG2 and U373 cells seeded on 24-well plates at the density 80 x 10^3 and 60 x 10^3 per well, respectively, 2 days before starting treatments. Cells were exposed to S29434 or vehicle (DMSO) for 6, 18 and 24

h before the end of the experiment. Next, the cells were washed with pre-warmed serum-free DMEM (high and low-glucose, depending on the cell type) and then incubated with MitoSox (2.5 µM, 15 min) diluted in DMEM as above. The experiment was finished by washing the cells twice with pre-warmed phosphate-buffer saline followed by trypsin-mediated detachment of cells and flow cytometry analysis according to a previously published protocols (Janda et al., 2013)

Transient silencing of QR2 expression and autophagy assay in hepatic cells. HepG2 cells, were cultured a sdescribed above. Cells were seeded on 12-well plates one day before transfection at a density of 30,000 cm^{-2}. Non-silencing or control (Ctrl) siRNA (All-stars) and a set of human QR2-targeting siRNA were purchased from Qiagen (Hilden, Germany). Transfection of HepG2 cells was performed using Lipofectamine 2000 (L2000, Life Technologies, Invitrogen, Monza MB, Italy) and Optimem (Life Technologies, Invitrogen) according to the manufacturer's instructions. Briefly, 360 pmol siRNA QR2 or control siRNA and 18 µl of L2000 were mixed and incubated in 600 µl of Optimem for 15–20 min at room temperature. Each well containing HepG2 cells in 500 µl of serum-free medium was overlaid with 100 µl of siRNA-Lipofectamine complexes and incubated in a cell-culture incubator. After 5 h, the medium was changed for DMEM supplemented with FBS without Pen-Strep. At 24 h later, the cells were treated with S29434 or DMSO for 24 h in regular medium with Pen-Strep. CLQ 25 µM was added 3 h before the end of the experiment to half of the samples. The cells were lysed, and the lysates were run on 12% SDS-PAGE gels and assayed for LC3 and QR2 expression by western blotting, as previously described (Janda et al., 2015). The antibodies were polyclonal rabbit anti-LC3A/B (MBL,Enzo Life Sciences, Farmingdale, NY, USA) used at 1:2000, anti–glyceraldehyde-3-phosphate dehydrogenase (Santa Cruz Biotech, Dallas, TX, USA) used at 1:500and anti-QR2 (Sigma-Aldrich) used at 1:1000).

Testing S29434 against neuronal degeneration in vitro. Animals were housed, handled, and taken care of in accordance with recommendations of the Guide for the Care and Use of Laboratory Animals of the National Institutes of Health (NIH Publication no. 85-23, revised 1996) and the European Union Council Directives (2010/63/EU). Experimental procedures were authorized by the ethical committee on animal experiments (Comité Charles Darwin #5). Cultures were prepared from the ventral midbrain of Wistar rat embryos at gestational age 15.5 days (Janvier LABS, Le Genest-St.-Isle, France). Dissociated cells in suspension obtained by mechanical trituration of midbrain tissue pieces were seeded at a density of 1.2–1.5 × 10^5 cells/cm^2 onto Nunc 48-well multi-dish plates precoated with 1 mg/mL polyethylenimine diluted in borate buffer, pH 8.3, as previously described (Toulorge et al., 2011). In some experiments, the cultures were maintained in N5 medium supplemented with 5 mM glucose, 5 % horse serum, and 0.5 % fetal calf serum, except for the first 3 days *in vitro*, when the concentration of fetal calf serum was set at 2.5 % to favor initial culture maturation (Guerreiro et al., 2008). In the other experiments, we used a chemically defined serum-free medium consisting of equal volumes of Dulbecco's minimal essential medium and Ham's F12 nutrient mixture (DMEM/F12, Life Technologies, Invitrogen), supplemented with 10 µg/mL insulin, 30 mM glucose, and 100 IU/mL Pen-Strep (Troadec et al., 2001). Dopamine neurons were detected by tyrosine hydroxylase immunofluorescence staining using procedures previously described (Toulorge et al., 2011). These neurons represented approximately 2-3% of the total number of neuronal cells present in these cultures after plating. The cultures, fixed for 12 min using 4% formaldehyde in Dulbecco's phosphate-buffered saline (PBS), were washed twice with PBS before an incubation step at 4 °C for 24 - 72 h with primary antibodies. A monoclonal anti- tyrosine hydroxylase antibody diluted 1/5000 (ImmunoStar, Inc., Hudson, WI, USA) or a polyclonal anti- tyrosine hydroxylase antibody diluted 1/1000 (US Biologicals, Salem, MA, USA) was used to assess survival of

dopamine neurons. Cell counting was performed with a Nikon TE 2000 inverted microscope (Nikon, Champigny-sur-Marne, France) at 200 time magnification, using a 20 × objective matched with a 10 × ocular. The number of tyrosine hydroxylase+ neurons in each culture well was estimated after counting visual fields distributed along the x- and y-axes. The functional integrity and synaptic function of dopamine neurons were evaluated by their ability to accumulate [^{3}H]-dopamine (50 nM; 40 Ci/mmol; PerkinElmer, Courtaboeuf, France), as previously described (Guerreiro et al., 2008). When using N5 medium supplemented with serum, dopamine neurons in culture degenerate spontaneously and progressively during the maturation process of these cultures (Toulorge et al., 2011). Thus, in this setting, pharmacological treatments were initiated immediately after plating and were then renewed daily after replacing a fraction (two thirds) of culture medium. Dopamine cell survival was assessed in 9 days in vitro cultures, i.e., at a stage where about 70 % of dopamine neurons have already died (Toulorge et al., 2011). Some sets of cultures were treated with veratridine (0.8 µM), a depolarizing agent used as a positive control for neuroprotection in this setting (Salthun-Lassalle et al., 2004). Treatments with the mitochondrial toxin MPP^+ (1-methyl-4-phenylpyridinium) were performed in cultures in which the spontaneous death process was prevented by supplementing the N5 medium with a depolarizing concentration of K^+ (30 mM) in the presence of 1 µM of the *N*-methyl-D-aspartate receptor antagonist dizocilpine ([5R,10S]-[1]-5-methyl-10,11-dihydro-5*H*-dibenzo[a,d]cyclohepten-5,10-imine, a.k.a. MK-801), as previously described (Salthun-Lassalle et al., 2004). Note that this treatment did not interfere with the neurotoxic effects of MPP^+. MPP^+ was applied to midbrain cultures between 4 and 6 days in culture, whereas protective treatments were added after 2 days in vitro culture and renewed thereafter until fixation of the cultures at 6 days in culture. Finally, oxidative stress–mediated dopamine cell death was achieved by placing the cultures in a defined serum-free DMEM/F12 medium containing 1.5 µM of ferrous iron (Troadec et al., 2001). The

antimitotic compound ARA-c (1.5 µM) was added to the cultures after plating to prevent glial cell proliferation. Dopamine cell survival was assessed at 5 days in culture in these conditions. Experimental values expressed as mean ± SEM were derived from triplicates of three independent experiments. Data were analyzed using the SigmaPlot 12.5 software (Systat Software Inc, San Jose, CA, USA) with one-way analysis of variance (ANOVA) followed the Student–Newman–Keuls post hoc test for all pairwise comparisons.

Object recognition in mice. Experiments were performed in a quiet, dimly lit room in a dark Plexiglas chamber (L × W × H: 25 × 35 × 25 cm). On the day before the test day (day 0, familiarization phase), the animals were allowed to explore the test apparatus for 2.5 min. Twenty-four hours later (day 1, acquisition phase), after a 30-min pretreatment time after drug treatment, each test animal was placed in the middle of the test box from the previous day, and the 5-min acquisition trial was begun. In the first trial, mice were allowed to explore two identical objects (10 sec per object within a total 5-min period). During test time, the exploration time (ET) was measured with a stopwatch. ET is defined as direct, active olfactory exploration of objects 1 and 2. In general, it consists of nosing and sniffing of the edge and the top, as well as approaching and crossing the line approximately 1 cm around the objects. Posturing and mounting are not included in measures of investigation. On day 2 (24 h later, retention phase), a new object and a familiar object were placed in the test box, and the animals were replaced in the box for 4 min and ET measured again. Discrimination index = [Exploration time of new object in seconds (N) – Exploration time of familiar object in seconds (F)]/[Exploration time of new object in seconds (N) + Familiar object exploration time in seconds (F)] = [N-F]/[N+F]. A thorough description of these methods can be found in previous publications (Ennaceur and Delacour, 1988; Bartolini et al., 1996; Bevins and Besheer, 2006). For in vivo data, one-way ANOVA was performed (followed by Dunnett's multiple comparisons test) for the DI data.

Results

Chemistry. S29434 was synthesized by Guillaumet and colleagues in the late 1990s as a compound to explore the melatoninergic system(s). We introduced the notion that it could be an interesting tool for QR2 studies after we discovered that MT3, the elusive and unconventional melatonin binding site we and others described (Duncan et al., 1988; Paul et al., 1999) was indeed QR2 (Nosjean et al., 2000). The first synthesis, as usual, aimed at producing several examples of tetracyclic chemicals that could be assimilated into two indolic structures fused together. The goal at that stage was to document the chemical series. The synthetic route is summarized in **Fig. 1**. The second synthesis scheme was intended to rationalize the yields of each step, even if alternative synthetic steps had to be substituted in the original protocols, as summarized in **Fig. 2**. Full details of the synthetic routes are given as supplementary data. Of key note, the final product, used in most of the experiments presented herein, is 99% pure, as can be seen from the analytical details given in the **supplementary data** section.

Inhibition of quinone reductase 2. Various reports from the literature show that, depending on the substrate/co-substrate couples used to measure the catalytic activity of QR2, the recorded IC50 values range from 1 to 40 nM as summarized in **Table 1**. We stabilized our system in a standard configuration (see materials and methods section) for all the internal needs for screening on this enzyme (during which S29434 was used as a reference compound) and ended up with an IC_{50} of 16 ± 3.2 nM (n = 51). The considerable amount of data accumulated on this material during several years render this information quite robust, at least using the human cloned enzyme, BNAH as co-substrate and menadione as substrate. A typical sigmoid curve of concentration/activity relationship is presented in **Fig. 3A**. We also present the comparison of the inhibition by S29434 of the enzyme catalytic activity while using BNAH, a synthetic co-substrate, or NRH, a natural candidate co-substrate of QR2 (**Fig. 3B**).

One can see that the inhibition using the natural co-substrate is slightly moved leftward, towards a more potent IC_{50} in the low 5 nM range. Nevertheless, the use of BNAH is recommended because the compound is commercially available and slightly more robust that its ribosylated counterpart (Boutin et al., 2005).

Inhibitor specificity: *Standard panel of molecular target*s (Eurofins-CEREP profiles). It was important to start as early as possible on checking the specificity of the inhibitor S29434. Our classical way of doing this was to check its activity in a series of standard assays designed to evaluate its behavior against a selection of receptors and enzymes [see, for example, Millan et al. (2012)]. All the tests were done in duplicate, independently, at two concentrations: 100 nM and 10 µM. None of these assays revealed a capacity of the compound to inhibit the binding at or the activity of those selected targets, even at fairly high concentrations (>10 µM) (data not shown). One notable exception is the capacity of S29434 to displace the binding of 2-iodomelatonin at the melatonin receptor MT2, for which the compound has an affinity of 0.14 µM, which is not surprising because the compound was initially synthesized as part of a melatonin receptor agonist discovery process. Finally, S29434 has no cytotoxic activities towards the following standard cancer cell lines Caco-2, HCT116, HT-29, and L1210 up to 10 mM.

Inhibitor specificity: *Kinases*. Duncan et al. (2008) reported the toxicity of two casein kinase 2 inhibitors: TBBz (4,5,6,7-1*H*-tetrabromobenzimidazole) and DMAT (2-dimethylamino-4,5,6,7-tetrabromo-1*H*-benzimidazole), presumably because of their inhibition of QR2 catalytic activity. Similarly, Rix et al, reported that the only non-kinase target of the BCR-ABL inhibitors, imatinib and nilotinib, was QR2 (Rix et al., 2007).Thus, we wanted to know if this QR2 inhibitor was able to inhibit one or several catalytic activities of a panel of kinases. Of the 46 different kinases of the panel, none was significantly (more than 20 %)

inhibited by S29434 at 100 nM (data not shown). Because of the high potency of S29434, no higher concentrations were tested.

Inhibitor specificity: *Quinone reductase 1*. The main component of a possible specificity for S29434 would be its activity with the closest relative of QR2, namely, QR1. Inversely, we wanted to confirm that the standard QR1 inhibitor (Ernster et al., 1962), dicoumarol, which has been widely used over the last decades, was not an inhibitor of QR2. Using the catalytic activity measurement of the enzymes, the comparison has been made in the past (Ferry et al., 2010), showing a good selectivity on pure enzymes of S29434 on QR2 over QR1 and vice-versa for dicoumarol. In a new set of experiments, (see **Fig. 4**), we show the absence of inhibition of QR1 by 10 µM of S29434 compared to the full inhibition by dicoumarol.

Inhibitor specificity: *sirtuin*. Because of the link between sirtuin-mediated NAD degradation (Jiang et al., 2017) and the use by QR2 of a possible catabolite of NADH, we wanted to make sure that the activity of the inhibitor did not lead to upstream inhibition of this enzyme, diminishing the availability of the co-substrate of QR2. Even at 10 µM, S29434 does not inhibit this enzyme while SOD or diphenyleneiodonium chloride are potently inhibiting sirtuin activity (not shown).

Inhibitor specificity: *NADPH oxidase*. In addition to mitochondria, a main cellular source of ROS production are NADPH oxidase(s) (Sorce et al., 2017; Teixeira et al., 2017). Thus we checked the capacity of S29434 to inhibit this family of enzymes. The test was assessed with the NOX inhibitor diphenyleneiodonium. While this reference compound led to a complete inhibition, S29434 remained poorly active up to 10 µM, at which point it began to inhibit about 20% of the ROS production from those cells (see **Supplemental Figure 3**).

S29434/quinone reductase 2 characteristics: *Binding kinetics*. Resveratrol has been described as a potent inhibitor of QR2 (Buryanovskyy et al., 2004) and thus might serve as a reference compound in some conditions. The binding of both compounds (S29434 and

resveratrol) leads to the quenching of the intrinsic fluorescence of QR2 (FADox). Pre-equilibrium stopped-flow spectroscopy was used to measure the real-time binding kinetics of the two compounds and compare their binding mechanism (**Fig. 5**). On one hand, resveratrol binding kinetics being too fast at 25°C, they were slowed-down by decreasing the temperature to 4 °C. Data were consistent with a single-step binding mechanism, governed by an association rate constant k1 of 19 10^6 s^{-1} M^{-1} and a dissociation rate constant k_{-1} of 27 s^{-1}. A K_D estimate of 1.4 µM was calculated from the ratio k_{-1}/k_1, which is in fairly good agreement with isothermal titration calorimetry (ITC) data obtained on the same enzyme batch, yielding a K_D of 0.6 µM at 25 °C (data not shown). On the other hand, S29434 displayed slower but biphasic binding transients, consistent with a two-step binding mechanism involving a conformational change. Re-plot of the k_{obs} rate constants for the fast phase yielded a linear plot, diagnostic of a bimolecular association step, governed by a k1 of 14 10^6 s^{-1} M^{-1} and a dissociation rate constant k_{-1} of 61 $s^{-1}.M^{-1}$. A K_D estimate for this encounter complex of 4.4 µM can be calculated from the ratio k_{-1}/k_1. The observed rate of the slow phase was independent of the S29434 concentration in the investigated range, staying close to 30 s^{-1}. This step is therefore likely reflecting a conformational rearrangement, either following binding (induced-fit) or preceding it (conformational selection). While preliminary, these kinetic data strongly suggest the evolution of the binding mechanism from the low-affinity single-step binder resveratrol to the high-affinity two-step binder S29434. They also are in agreement with results from our mass spectrometry studies of the inhibitor/enzyme binding (Antoine et al., 2012).

S29434/quinone reductase 2 characteristics: *Pause of S29434 in QR2*. S29434 has been co-crystallized in QR2 on several occasions (Pegan et al., 2011; Gerard et al., 2018), but its pause inside the crystal was poorly discussed. In brief, as shown in **Fig. 6**, the ligand S29434 fits deeply into a QR2 hydrophobic cavity (PDB: 3OX3), interacting with both subunits A and B

with its amido-furan side chains pointing toward the solvent. It makes π-edge interactions with Trp105 and Phe126 π-π interactions with Phe178 and a water-mediated H-bond with Asn161. Additional π-π interactions exist with co-factor FAD. Although the furan moiety makes an additional hydrophobic interaction with Ile194 from QR2, it also seems that this part of the molecule somehow hangs out of the catalytic site, potentially offering the possibility to modify/decorate this part of the molecule with associated properties, as for instance a fluorophore moiety.

Notions of S29434 drug metabolism. As often happens, at this stage of the research programs, some experiments were conducted to better understand the properties of the compound in terms of pharmacokinetics or more generally from the drug's cellular penetration. The first experiments were those involving measurement of the behavior of S29434 in an *in cellulo* blood-brain barrier model (Cechelli et al., 1999), based on co-cultures of bovine brain micro-vessel endothelial cells and rat astrocytes (Booher and Sensenbrenner, 1972). We measured the permeability surface total (PSt) (filter + collagen + cells) and the permeability surface filter (PSf) (filter + collagen without cells) expressed in milliliters per minute. These values were 4.58 cm/min and 3.78 cm/min, respectively. Therefore, the ratio PSt/PSf (permeability class) for S29434 was determined to be 121%, classifying it into the high category of permeable compounds.

Reactive Oxygen Species and quinone reductase 2: *QR2-mediated ROS production*. QR2 activity can be followed by EPR (Reybier et al., 2011; Cassagnes et al., 2015). As stated above, this functional assay is indirectly linked to the enzyme. Indeed, the product of the reaction, a quinol, has a poor stability in standard conditions. Thus, in the presence of oxygen, the quinol is oxidized back in the original quinone which in turn serves as substrate for the enzyme, starting a futile cycle between the two chemical species with the concomitant production of reactive oxygen species [see Reybier et al (2011) for complete discussion]. This

process seems to occur in a-cellular as well as in cellular contexts (Cassagnes et al., 2017). Here, we completed and reinforced these data by showing by EPR spectroscopy that pure QR2, in the presence of its co-substrate (BNAH), produces ROS during the catalytic activity (**Fig. 7**) that is inhibited by S29434. Furthermore, under those experimental conditions, neither NADH nor NAD(P)H can substitute for BNAH. Note that in basal conditions (no substrate and co-substrate of QR2), very low levels of ROS were recorded.

Reactive Oxygen Species and quinone reductase 2: *Mitochondrial respiration in liver and brain*. Because S29434 diminishes the amount of ROS produced during the futile cycle between quinol and quinone in aerobic conditions (Reybier et al., 2011), we wanted to make sure that this effect was not the result of some direct interference of S29434 with ROS even though the compound is inactive in other ROS-generating systems (such as mitochondria). Thus, it was confirmed that S29434 cannot trap hydroxyl radicals ($^{\bullet}OH$) produced via the Fenton reaction or superoxide radicals ($O_2^{\bullet-}$) produced from crown ether and KO_2 (not shown). Furthermore, another source of cellular ROS production was tested: the mitochondria-mediated production of radical species. To evaluate the mitochondrial effect of drugs, mitochondrial respiration was settled with complex I substrates (glutamate/malate) and in phosphorylating conditions (1.25 mM ADP). The relative effect of increasing amounts of S29434 is indicated by the ratio of respiratory rates compound/solvent, with a value of 1 indicating a lack of effect. With this approach, S29434 did not produce a significant effect at concentrations up to 10 µM and revealed no statistically significant changes in respiratory rate with rat liver or rat brain mitochondria (**Fig. 8**). The system was validated with experiments with rotenone or oligomycin, two known inhibitors of the mitochondrial respiratory chain, leading to results similar to those reported in the literature (data not shown).

Reactive oxygen species and quinone reductase 2: *Mitochondrial respiration in muscle.* Thorough studies were then independently conducted on mitochondria in saponin-

permeabilized rat gastrocnemius muscle fibers. As illustrated in **Fig. 9 A**, no differences in respiration were observed between conditions, confirming that neither BNAH nor S29434 affected respiration in these samples. Likewise, BNAH and S29434 did not affect H_2O_2 production (**Fig. 9 B**). When H_2O_2 was expressed as a percentage of O_2 flux, a significant difference was observed between the BNAH and BNAH + S29434 (**Fig. 9 C**) only in the absence of ADP, suggesting that BNAH may increase mitochondrial H_2O_2 in non-phosphorylating (i.e., State 4, or LEAK) conditions. However, because neither respiration nor H_2O_2 alone was affected, a more plausible explanation is that the difference in proportional H_2O_2 production is the result of non-mitochondrial sources of H_2O_2 in the samples and not of bulk O_2 flux.

Effects of S29434 on cells. *Nervous system cells*. S29434 was described to have a beneficial effect against paraquat-induced toxicity *in cellulo* and *in vivo* (Janda et al., 2013; Janda et al., 2015), suggesting a potential role of QR2 in Parkinson's disease. This prompted us to analyze its effect in models of neuronal degeneration *in cellulo*. To this aim, primary midbrain dopamine neurons in culture have been established from fetal rat ventral midbrains. S29434 (up 100 µM) could not reduce the spontaneous loss of dopamine neurons in culture (**Fig. 10 A**), while the reference neuroprotective molecule, veratridine, efficiently rescued these cells. S29434 also failed to protect dopaminergic cells from iron-induced oxidative stress, (in presence of iron in the culture medium) caused by Fenton-type reaction occurring spontaneously (**Fig. 10 B**). At 100 µM, there was even a tendency for S29434 to become slightly toxic. However, as expected, the chelation of iron with deferoxamine (10 µM) afforded a robust protection under these conditions. In contrast to what we observed in the two previous settings, S29434 showed concentration-dependent protective effects against the mitochondrial complex I inhibitor MPP^+ (**Fig. 10 C**). The effect of S29434 was already significant at 0.1 µM, peaked at 1 µM, and declined progressively between 10 and 100 µM.

Dopamine cell rescue was also observed with the positive control, nicotine, used at 10 µM. Because MPP^+ is selectively taken up by the dopamine transporter to exert its selective toxicity towards dopamine neurons, we tested whether S29434 was operating as an inhibitor of dopamine uptake. This was not the case because S29434 does not bind to the ad hoc transporter (not shown) strongly suggesting that S29434 was blocking the intrinsic mechanism of toxicity of MPP^+.

Effects of S29434 on cells. *Autophagy*. Autophagy is a vesicle-mediated pathway that ensures the recognition and transport of defective organelles and protein aggregates to lysosomes, where they are digested. We tested if S29434 could induce autophagy, in the human HepG2 cells, derived from liver, the organ with the highest level of QR2 expression (Nosjean et al., 2000). S29434 dose-dependently induced LC3-II, a marker of autophagy vesicles (**Fig. 11A**). Silencing of QR2 by more than 50% increased basal LC3-II levels and suppressed LC3-II induction by S29434, indicating that the autophagy response to this compound does not depend on its off-target effects, but it is directly mediated by QR2 inhibition (second panel in **Fig. 11 A & B**). Of importance, LC3-II was further accumulated in S29434-treated cells, when autophagy flux was blocked by the lysosomal inhibitor ClQ, indicating a true induction of autophagy by the QR2 inhibitor (**Fig. 11 B)**. Further details are given, including the comments on the whole blots as **Supplementary Data 8**. These data confirm that QR2 plays a role in regulation of autophagy. Oxidative stress and redox reactions have a strong impact on autophagy machinery (Janda et al., 2012; Janda et al., 2015). However, since QR2 inhibition does not reduce basal ROS levels neither in HepG2 cells (**Fig. 12A**), nor in U373 astrocytes (**Fig. 12B**), the mechanism by which S29434 triggers autophagy should be mitochondrial ROS-independent and QR2-dependent as suggested by the data presented above (**Fig. 11A & B** and **Supplementary Data 8**).

Effects of S29434 *in vivo*. *Object recognition tests in CH3 wild-type mice*. The interplay between QR2 and "memory" has been observed in several occasions (Brouillette and Quirion, 2008; Benoit et al., 2010; Rappaport et al., 2015). Thus, we wanted to document further this relationship, using the inhibitor S29434 in the object recognition test. The test trial with the new object was carried out 24 h after the acquisition trial with two identical objects. S29434 was given intraperitoneally, 30 min before the acquisition trial. The discrimination index is shown, where N is the time spent inspecting the new object, and F is the time spent exploring the familiar object during the test trial (**Fig. 13A**). Both concentrations of S29434 led to an enhanced time of exploration of the unfamiliar object. Under these circumstances and experimental conditions, the object recognition memory of wild-type mice is fairly enhanced by the treatment. As other authors working with other models have reported (Rappaport et al., 2015), this finding suggests that the compound, by inhibiting QR2, has a positive effect on at least this particular aspect of memory.

***In vivo* considerations on S29434**. *Object recognition memory in the KO CH3QR2$^{-/-}$ mice*. The same experiments were carried out on KO CH3QR2-/- mice. The corresponding results are presented in **Fig. 13 B**. For QR2 KO animals, the results strongly reinforce the previous experiments. Indeed, the treated (1 or 15 mg/kg) and control animals did not differ, indicating that the product has no further effect on this parameter. Because the QR2 KO animals were genetically deficient only in this enzyme (Mailliet et al., 2004), this lack of activity of S29434 strongly suggests that the compound is specific to QR2. Furthermore, we know these animals did not lose their learning capacity compared to the wild-type mice as demonstrated in several tests including the Morris water maze, object recognition, and rotarod performance test. All their performances in those tests were superior to those by their wild-type counterparts (Benoit et al., 2010).

Discussion

General. Molecular pharmacology is based on either the manipulation (including the mutagenesis) of targets or their inhibition/activation by synthetic or natural chemicals. Hundreds of compounds have been described to serve such tasks. Using those tools, it is possible to better understand the mechanisms by which targets (receptors, enzymes) regulate physiological systems, up to a point where pathology replaces physiology and drugs replace chemicals. This naïve way of describing what is the basis of Pharmacology and thus of Therapeutics permits to better understand the limits of those approaches. Indeed, finding a compound is not usually complicated, and the modern use of high-throughput screening campaigns together with the power of the virtual analyses led very often to compounds that interact with a target in a given system. Obviously, going from chemicals to drug involves many aspects that are often complicated obstacles to overcome. A way to clarify the future use of a new compound is to deliver as many information as possible on it. In an area not distant from QR2 pharmacology, a good counterexample is certainly dicoumarol, the QR1 reference inhibitor. This compound has been widely used in the literature (over 2700 references) and still, many of its off-targets effects biases the interpretation of the data obtained with this compound [see discussion in Scott *et al* (2011)].

For many reasons, the project to which S29434 was originally attached (melatoninergic ligands) led us to quinone reductase 2 and a completely different avenue of research, as described elsewhere (Boutin, 2016). By distributing the compound to colleagues looking for the role of this curious enzyme in various systems, we did not follow the best path. Indeed, no information was available at that time on the various situations in which the compound was tested: *in cellulo* or *in vivo*. The stability, permeability and overall specificity of S29434 were among the information that we did not know. Furthermore, no clear synthesis method was

published so far. We thus decided to complete the already available information on S29434 by bringing either completely new or by reinforcing previously but minimally documented findings.

Chemistry. S29434 belongs to a family of flat tetracyclic compounds some of which were described by us (Boussard et al., 2006) or by others: cryptolepines (Onyeibor et al., 2005; Lavrado et al., 2008; Whittell et al., 2011) or other types of indolizino-indolones (Bhattacharya et al., 2001) for different purposes. Compounds known to inhibit QR2 activity were also reported in the literature, such as pyrroloquinoline ammosamides (Reddy et al., 2011), or furan-amidines (Alnabulsi et al., 2018). A few, if any, were tested and documented outside their enzymatic test activities, thus we believe that the present report is remarkable because it described S29434 in different *in cellulo* as well as *in vivo* situations.

Acellular behavior, *specificity*: In an a-cellular system, the compound is a potent inhibitor of the activity of the QR2 2. It does not or only marginally inhibit QR1. Furthermore, among more than a hundred other targets, it does not potently interfere with any, with the sole exception of the melatonin receptor 2 for which it has a binding affinity in the micromolar range. Of course, the notion of specificity is limited to the targets the measures of which are available. Indeed, it is impossible to know if the compound will uniquely recognize QR2 among the protein products of the 26 000 genes of the human genome. The mechanism by which S29434 binds to and interacts with QR2 has been scrutinized at several occasions (Pegan et al., 2011; Antoine et al., 2012). Here, we bring more information on the way the compound fills up the catalytic site of the enzyme, with trends on how this can be further accomplished, as well as a way to measure the affinity of the compound for the enzyme, in complement to its capacity to inhibit it. These two notions (affinity for an enzyme and inhibition potency) are too often mixed up. It is important to be able to segregate between the affinity with which the compound recognizes the enzyme and its capacity to impair its

activity. Furthermore, the first of those biophysical measures permits to evaluate the time of residency during which the compound stays inside the catalytic site. This time can widely vary inside a series of analogue compounds for a given enzyme ranging from seconds to hours. The implication of this measure is the time during which the compound stays in the enzyme.

Stability in vivo*, membrane crossing.* S29434 seems to be fairly stable in animal experiments, based on previously published data on S29434 (Benoit et al., 2010; Janda et al., 2013; Janda et al., 2015) as well as the study on its blood-brain barrier crossing provided here. Based on several published observations, it was already clear that the compound was penetrating very different types of primary or cultivated cells (Benoit et al., 2010; Janda et al., 2013; Chen et al., 2017). It was also clear that because the compound was active in rodent models, administered by intraperitoneal (Janda et al., 2015; Rappaport et al., 2015) or by intra-cerebroventricular (Janda et al., 2013) routes, it should be fairly stable in mammals and that sufficient quantities were reaching the brain. Indeed, in each case, the effects seen *in vivo* could have been interpreted as an inhibition of QR2, strongly suggesting stability and penetration.

Cellular aspects, reactive oxygen species. As explained, there is a crucial link between QR2 and ROS production. Thus, our main goal was to ensure that the compound was not a scavenger *per* se, and that its capacity to diminish ROS bursts in cellular experiments was due only to its interference with QR2. Indeed, experiments conducted on cells show that the compound is capable to inhibit QR2-dependent production of ROS in cellular experiments, on various types of cells such as hepatoma HepG2 cells, the astroglial cell line U373, (Janda et al., 2013) as well as on primary dopaminergic neurons (Cassagnes et al., 2017). However, the compound does not alter basal ROS levels in cells when applied in the absence of exogenous QR2 activators. For example, we treated HepG2 and U373 cells with S29434 at 6, 18, and 24

h before measuring the intracellular ROS levels with MitoSox, a fluorescent compound recognizing preferentially mitochondrial superoxide anion (Polster et al., 2014). MitoSox fluorescence was unaltered by S29434 at all experimental times in HepG2, while an unspecific antioxidant, *N*-acetyl cysteine (NAC), significantly reduced basal ROS levels (Fig. 12). Mitochondria are the main source of cellular ROS in physiological conditions. It was thus important to conduct detailed studies on mitochondria from various organs and to validate that in all conditions, S29434 was not able to inhibit this ROS production. Furthermore, it does not inhibit Nox, nor it impairs ROS produced from a Fenton-type reaction to be toxic to neuronal cells. These data strongly suggest that S29434 is specific of QR2.

Cellular aspects, autophagy. The autophagy pathway mitigates the cellular damage that occurs in response to stress and toxic agents and plays an important role in ensuring basal protein and organelle turnover (Janda et al., 2012; Dagda et al., 2013). While studying the antioxidant effects of S29434 on paraquat-induced toxicity, we discovered that this compound has yet another property, which is the ability to restore basal autophagy in paraquat-treated astrocytes. In addition, we found that S29434 induces autophagy in the absence of paraquat and that this response was mediated by a QR2-dependent mechanism in astrocytes (Janda et al., 2015). The data presented in the present work indicate that QR2-dependent mechanism of autophagy induction can be generalized to other cell types such as liver cells. Furthermore, we show here that this effect does not correlate with any detectable modulation of ROS levels in liver cells, thus excluding possible ROS-dependent basis of the pro-autophagic activity of S29434. The accumulation of LC3-II in the presence of ClQ is believed to result from a blockade of lysosome activity, but it might partially depend on the ability of the anti-malaria drug ClQ to bind and inhibit QR2 directly, although with a poor affinity when compared to S29434 (Kwiek et al., 2004; Leung and Shilton, 2015). Indeed, a direct effect of ClQ on QR2

is much weaker than its inhibitory effect on lysosomal digestion because LC3-II still accumulates when QR2 expression is reduced by siRNA (Fig. 11 B, compare lines 1 and 4).

Cellular aspects, neuronal cells. Another key result is presented here. MPP^+, the active metabolite of MTPT, is an inhibitor of the mitochondrial complex I. This compound once delivered to mice, leads to a Parkinson-like syndrome. We know that QR2 does not recognize MPTP as a substrate; nevertheless, S29434 provides a concentration-dependent protection in this model. Of interest, paraquat and MPP^+ are both Parkinsonian toxins and share common toxicity mechanisms, including the inhibition of complex 1 activity in the mitochondria and dysregulation of autophagy (Dagda et al., 2013).

In vivo activity, ultimate specificity. Of course, one of the possible ultimate proofs of specificity would be in a case were an enzyme activity is linked to a clear observation (for instance, memory or certain type(s) of memory) in vivo. In that case, assuming or proving a reasonable penetration, distribution and stability of a compound, if this compound is active – inhibiting the activity – in wild type mice and inactive on the same parameter in knock-out mice for this particular protein, one can assume, once again, a higher degree of specificity of the molecule. It is exactly the situation we described herein: wild type mice in object recognition memory test are sensible to S29434: after treatment, mice are spending an enhanced period of time exploring the unfamiliar object compared to the untreated mice, suggesting also a role of QR2 in memory after others (Harada et al., 2001; Benoit et al., 2011; Rappaport et al., 2015). Finally, the same experiments in engineered mice in which QR2 has been deleted, the compound is not active anymore. Of note, since the first observation (Brouillette and Quirion, 2008), it seems that the QR2 catalytic activity aims at suppressing several types of memory, potentially linked to dopaminergic neurons (McNab et al., 2009; Rossato et al., 2009; Nobili et al., 2017), see also review by D'Amelio et al (2018).

The present paper does not cover the actions of S29434 in various models on inflammation, that are often linked to ROS production, but S29434 does not influence Toll-like receptors or inflammasome signaling (Groß et al., 2016) as an activator or inhibitor (O. Gross, personal communication). Further work is needed to better understand a possible role of QR2 in inflammation responses.

In summary, S29434 is a powerful inhibitor of QR2. It is specific over QR1 and over a range of standard pharmacological targets. It is fairly stable *in vivo*, and penetrate cells. Nevertheless, the body of results gathered in the present work does not guarantee the specificity of S29434 but clearly delineates some of its actions, and particularly in various models that help confirming that its actions are largely the result of its capacity to powerfully inhibit QR2. Several other molecules have been described as inhibiting QR2, such as resveratrol, melatonin, and some flavonoids, but they are non-specific and inhibit many different enzymes in many different pathways; thus, using them to dissect a given pathway is difficult. As such, we believe that the present work lays a strong foundation for the pharmacological use of S29434 in many situations to evaluate the role of QR2.

Acknowledgments: JAB wishes to thank Dr. Hemal Soni (O2h, Ahmedabad, India) for his help in writing the second chemical part, San Francisco Edit for their help in editing and rewriting this manuscript, and finally Drs. Philippe Delagrange (Servier, Croissy-sur-Seine, France), Nathaniel Gould & Kobi Rosenblum (Haifa, Israel) and Olaf Gross (München, Germany) for their intellectual contributions. E. Hirsch and P. Michel acknowledge the support of the funding programs "Investissements d'avenir" ANR-10-IAIHU-06 and "Investissements d'avenir" ANR-11-INBS-0011-NeurATRIS: Translational Research Infrastructure for Biotherapies in Neurosciences. This work benefited from equipment and services from the CELIS core facility (Institut du Cerveau et de la Moelle Epinière, Paris). We thank Cécile Bureau and Laetitia Da Costa for their technical help. Dr. D.A. Kane acknowledges support from the Canada Foundation for Innovation and the Natural Sciences and Engineering Research Council of Canada. Drs. D.A. Kane and K. Brebner thank Mackenzie Bell, Laura Davidson, and Helen Elizabeth Wallace for their technical assistance. Dr. E. Janda received financial support from Herbal and Antioxidant Derivatives *srl*, Biano (RC), Italy and from FFARB 2017 (Basic Research Activities Fund) and wishes to thank Dr. Concetta Martino (UMG Catanzaro, Italy) for technical assistance.

Authorship Contributions: Jean A. Boutin and Gilles Ferry conceived the project, organized the paper, and wrote the introduction and discussion. Mathias Antoine, Philippe Dupuis, and Johann Stojko developed and ran the enzymology experiments, wrote the related materials and methods and the results, and designed the corresponding figures. Marc Bertrand and Thierry Le Diguarher developed and ran the drug metabolism experiments and wrote the related materials and methods and the results. Frederic Bouillaud, Hala Guedouari, Karen Brebner, and Daniel A. Kane designed and ran the mitochondria experiments, wrote the related materials and methods and the results, and designed the corresponding figures. Marie-

Claude Viaud-Massuard, Hervé Da Costa, and Gérald Guillaumet conceived the molecule, synthesized it, wrote the related chemical materials and methods section, and developed the related figures. Vishalgiri Goswami and Aakash Patel conceived the alternate synthetic route, applied it to the synthesis of the molecule, wrote the related chemical materials and methods section, and developed the related figures. István Gacsalyi ran the in vivo experiments, wrote the related materials and methods section and the results, and designed the corresponding figures. Adeline Giganti and Jérôme Paysant designed and ran the specificity experiments, wrote the related materials and methods section and the results, and designed the corresponding figure. Pierre Ducrot ran the molecular modeling experiments, wrote the related results, and designed the corresponding figure. Etienne C. Hirsch and Patrick P. Michel designed and ran the neuron experiments, wrote the related materials and methods section and the results, and designed the corresponding figure. Elzbieta Janda designed and ran the autophagy experiments and flow cytometry ROS measurements, wrote the related results and materials & methods sections, and designed the corresponding figures. Monivan Chhour, Françoise Nepveu and Karine Reybier designed and ran the EPR and ROS experiments, wrote the related materials and methods section and the results, and designed the corresponding figures.

Figure Legends

Fig. 1: Schematic representation of the synthesis of S29434. Note that the yield presented here is not to be taken for the purity of the final compound(s) that were usually above 95 %.

Fig. 2: Schematic representation of an alternate synthesis of S29434. Note that the yield presented here is not to be taken for the purity of the final compound(s) that were usually above 95 %.

Fig. 3: Quinone reductase 2 inhibition by S29434. A) Inhibition profile of S29434 on pure quinone reductase 2. The pure enzyme (2 nM) was incubated with 100 µM of BNAH and 100 µM of menadione in a buffer consisting of 1 mM n-octyl-beta D-glucopyranoside in 50 mM Tris-HCl, pH 8.5 and 500 nM FAD. In the absence of enzyme, the reduction does not occur. **B**) Inhibition profile of the compound S29434 as a function of hQR2 co-substrate. IC50 values were here assessed in a standard enzymatic assay (Tris-HCl 50mM pH 8.5, FAD 500nM, n-octyl-B-d-glucopyranoside 1mM, DMSO 5%) consisting in 0.5nM E.coli expressed human QR2 (PDB: 2QX4) preincubed with S29434 [50pM - 5µM], either BNAH or NRH 100µM and triggered by addition of menadione 100µM. Results are expressed as % inhibition of the control activities deduced from BNAH (350nm) or NRH (340nm) absorbance measurements, and are the mean of 3 independent experiments.

Fig. 4: Specificity of S29434 towards quinone reductase 1. Comparison with dicoumarol. Reactive oxygen species production recorded with purified QR1 (5 µg/mL) in the presence of NADH (100 µM) and menadione (100 µM) once pre-incubated with buffer (control), S29434 (10 µM) or dicoumarol (10 µM). The corresponding EPR spectra are presented on the right panels. The production of ROS was evaluated by the double integration of the EPR spectra obtained with DMPO (50 mM) as spin-trap.

Fig. 5: **Binding kinetics of resveratrol and S29434 to QR2 (FADox). A, B, C**) Resveratrol. **D, E, F**) S29434. **A**) Fluorescence transients measured after mixing QR2 and resveratrol at 4°C, final concentrations were 1 µM and 8 µM, respectively. **B**) Residuals of the mono-exponential fit. **C**) Re-plot of the kobs values overlaid with the corresponding linear fit. **D**) Fluorescence transients measured after mixing QR2 and S29434 at 25°C; final concentrations were 1 µM and 8 µM, respectively. **E**) Residuals of the bi-exponential fit. **F**) Re-plot of the kobs values for the fast (upper plot) and slow (lower plot) phases. The fast-phase plot is overlaid with the corresponding linear fit.

Fig. 6: **Co-crystallization of S29434 with quinone reductase 2. A**) QR2 molecular surface colored by lipophilicity (blue: hydrophilic regions, green: hydrophobic regions). Ligand S29434 (coral, space filling model). **B**) Ligand S29434 binding cavity (orange: chain 1; pink: chain B; coral: ligand; lipophilic surface). **C**) Left: QR2/S29434 interactions; right: QR2/S29434 interactions with FAD (grey).

Fig. 7: **Effect of co-substrate and inhibitor on the QR2-dependent production of ROS.** *Left panel*: ROS production recorded with purified QR2 (25.6 µg/mL) and different co-substrates: BNAH, NADH or NAD(P)H, in the presence or not of 20 µM S29434. The production of ROS was evaluated by the double integration of the EPR spectra obtained with DMPO (50 mM) as spin-trap.*Right panel:* Crude EPR spectra recorded with BNAH or NADH and menadione.

Fig. 8: **Effect of S29434 on respiration of rat liver and brain mitochondria.** Rat liver mitochondria (**A, B**) and rat brain mitochondria (**C, D**) oxygen consumption was measured simultaneously in the two chambers of the respirometer O2k (www.oroboros.at). Successive additions are indicated below the X-axis (time). Firstly, (left to the vertical dotted line) we settled a fast respiring phosphorylating state by addition of substrates glutamate/malate (GM) and ADP. Then, (right to the dotted line) four additions of increasing concentrations (10^{-7} to

10^{-4} M) of S29434 were made (black line and empty dots) as a control same volumes of solvent (DMSO) were added (grey line). **A, B**: mean value of the oxygen consumption rate [in pmol/(s. mg protein)] * $p < 0.05$ with a paired t-test to compare the oxygen consumption rate with S29434 (100 µM) or solvent for the same period of time. **C, D**: ratio between the rates S29434/Solvent.. ** $p < 0.01$ with the Mann–Whitney rank test (http://vassarstats.net/) for the comparison of the ratio observed with S29434 at 10^{-4} with each of the others comparable situations (ADP and no further addition, S29434 10^{-7} to 10^{-5} M).

Fig. 9: **Effects of S29434 on mitochondrial respiration or H2O2 production in permeabilized skeletal muscle.** Saponin-permeabilized rat red gastrocnemius skeletal muscle fibers were incubated in the following prior to assay: 100 µM BNAH, 30 µM S29434, 100 µM BNAH + 30 µM S29434, or control (vehicle: 18.75 µl DMSO). Subsequently, respiration was measured in all conditions (**A**), and H_2O_2 in S29434 and BNAH + S29434 conditions (**B**). H_2O_2 as a percentage of O_2 consumed was also calculated. *$p < 0.05$, **$p < 0.01$, $n = 7$.

Fig. 10: **S29434 effects on neuronal cell cultures. A**) S29434 does not protect DA neurons that degenerate spontaneously in midbrain cultures maintained with serum-supplemented N5 medium. The effect of S29434 against cell death was tested at the concentrations indicated above. The reference compound is veratridine (VERA; 0.8 µM). *$p < 0.05$ vs. corresponding controls. **B**) S29434 does not protect DA neurons that degenerate from oxidative stress in midbrain cultures maintained with a chemically defined medium containing catalytic iron. S29434 was tested at concentrations indicated above. The reference compound was deferoxamine (DESF; 10 µM). *$p < 0.05$ vs. corresponding controls. **C**) S29434 protects DA neurons against MPP+-induced cell death. Survival of TH^+ neurons in midbrain cultures treated (open bars) or not with MPP^+ at a concentration of 3 µM. The effect of S29434 against MPP+-induced cell death was tested at concentrations indicated above. Reference compound is nicotine (Nic; 10 µM). *$p < 0.05$ vs. corresponding controls.

Fig. 11: **Induction of autophagy by S29434 in HepG2 cells is QR2-dependent.** HepG2 cells were transfected with 100 µM siRNA against QR2 or non-targeting siRNA (negative control). The following day, cells were treated with S29434 (5 and 10 µM) or vehicle (DMSO) for 24 h. (**B**) Lysosomal function inhibitor chloroquine (25 µM) or vehicle (water) (**A**) was added to duplicate experimental points 2.5 h before the lysis and analysis of LC3 levels by western blot (SDS-PAGE 12%). Optical density (OD) relative to loading control (glyceraldehyde-3-phosphate dehydrogenase) was analyzed for LC3-II and normalized to control DMSO-treated cells for chloroquine-treated and untreated samples, separately.

Fig. 12: **S29434 has no effect on basal mitochondrial ROS levels in cells.** Subconfluent **A**) human hepatoma (HepG2) and **B**) astrocytoma (U373) cell lines were treated with S29434 (10 µM), N-acetylcysteine (5 mM) or vehicle (DMSO) for 6, 18, and 24 h before analysis. ROS levels were determined by flow cytometry after staining with MitoSOX. The graphs show the mean ± SEM from three independent experiments performed at least in triplicate. Statistical analysis two-way ANOVA, followed by Tukey post-test, time versus pharmacological treatment, 3 groups per 3 times, n = 3 or 4 samples each group, **, $p < 0.01$ when compared to control at the same time point.

Fig. 13: **Effect of S29434 in vivo on object recognition memory**. **A**) Object recognition memory is enhanced by S29434 in wild-type mice. The test trial with the new object was carried out 24 h after the acquisition trial with two identical objects. S29434 was given intraperitoneally 30 min before the acquisition trial. The discrimination index (DI) is shown where N is the time spent inspecting the new object and F is the time spent exploring the familiar object during the test trial. Data are mean ± SEM, n = 9–10/group. *** $p < 0.001$, one-way ANOVA followed by Dunnett's test vs. medium-treated control animals (0 mg/kg) group. **B**) Lack of effect of S29434 on object recognition memory in CH3QR2-/- mice. The test trial with the new object was carried out 24 h after the acquisition trial with two identical

objects. S29434 was given intraperitoneally 30 min before the acquisition trial. The discrimination index (DI) is shown where N is the time spent inspecting the new object and F is the time spent exploring the familiar object during the test trial. Data are mean ± SEM, n = 10/group. ** $p < 0.01$ one-way ANOVA followed by Dunnett's test *versus* medium-treated control animals (0 mg/kg) group.

References

Alnabulsi S, Hussein B, Santina E, Alsalahat I, Kadirvel M, Magwaza RN, Bryce RA, Schwalbe CH, Baldwin AG, Russo I, Stratford IJ, and Freeman S (2018) Evaluation of analogues of furan-amidines as inhibitors of NQO2. *Bioorganic & Medicinal Chemistry Letters* **28:**1292–1297 doi: 10.1016/j.bmcl.2018.03.025.

Antoine M, Marcheteau E, Delagrange P, Ferry G, and Boutin JA (2012) Characterization of cofactors, substrates and inhibitor binding to flavoenzyme quinone reductase 2 by automated supramolecular nano-electrospray ionization mass spectrometry. *International Journal of Mass Spectrometry* **312:**87–96 doi: 10.1016/j.ijms.2011.07.011.

Bartolini L, Casamenti F, and Pepeu G (1996) Aniracetam restores object recognition impaired by age, scopolamine, and nucleus basalis lesions. *Pharmacol Biochem Behav* **53:**277–283.

Benoit CE, Bastianetto S, Brouillette J, Tse Y, Boutin JA, Delagrange P, Wong T, Sarret P, and Quirion R (2010) Loss of quinone reductase 2 function selectively facilitates learning behaviors. *J. Neurosci.* **30:**12690–12700 doi: 10.1523/JNEUROSCI.2808-10.2010.

Benoit CE, Rowe WB, Menard C, Sarret P, and Quirion R (2011) Genomic and proteomic strategies to identify novel targets potentially involved in learning and memory. *Trends Pharmacol. Sci.* **32:**43–52 doi: 10.1016/j.tips.2010.10.002.

Bevins RA and Besheer J (2006) Object recognition in rats and mice: A one-trial non-matching-to-sample learning task to study 'recognition memory'. *Nat. Protoc.* **1:**1306–1311 doi: 10.1038/nprot.2006.205.

Bhattacharya G, Su T-L, Chia C-M, and Chen K-T (2001) Synthesis and Autoxidation of New Tetracyclic 9 H ,10 H -Indolizino[1,2- b]indole-1-ones. *J. Org. Chem.* **66:**426–432 doi: 10.1021/jo001020m.

Bian J, Li X, Xu L, Wang N, Qian X, You Q, and Zhang X (2017) Affinity-based small fluorescent probe for NAD(P)H: Quinone oxidoreductase 1 (NQO1). Design, synthesis and pharmacological evaluation. *Eur. J Med. Chem.* **127:**828–839 doi: 10.1016/j.ejmech.2016.10.062.

Bindoli A, Rigobello MP, and Galzigna L (1990) Reduction of adrenochrome by rat liver and brain DT-diaphorase. *Free Radic. Res Commun.* **8:**295–298.

Bolton JL, Trush MA, Penning TM, Dryhurst G, and Monks TJ (2000) Role of quinones in toxicology. *Chem Res Toxicol* **13:**135–160.

Booher J and Sensenbrenner M (1972) Growth and cultivation of dissociated neurons and glial cells from embryonic chick, rat and human brain in flask cultures. *Neurobiology* **2:**97–105.

Boussard MF, Truche S, Rousseau-Rojas A, Briss S, Descamps S, Droual M, Wierzbicki M, Ferry G, Audinot V, Delagrange P, and Boutin JA (2006) New ligands at the melatonin binding site MT(3). *Eur. J Med. Chem.* **41:**306–320 doi: 10.1016/j.ejmech.2005.12.002.

Boutin JA (2016) Quinone reductase 2 as a promising target of melatonin therapeutic actions. *Expert. Opin. Ther. Targets.* **20:**303–317 doi: 10.1517/14728222.2016.1091882.

Boutin JA, Chatelain-Egger F, Vella F, Delagrange P, and Ferry G (2005) Quinone reductase 2 substrate specificity and inhibition pharmacology. *Chem. Biol. Interact.* **151:**213–228 doi: 10.1016/j.cbi.2005.01.002.

Brouillette J and Quirion R (2008) Transthyretin: A key gene involved in the maintenance of memory capacities during aging. *Neurobiology of Aging* **29:**1721–1732 doi: 10.1016/j.neurobiolaging.2007.04.007.

Buryanovskyy L, Fu Y, Boyd M, Ma Y, Hsieh T-c, Wu JM, and Zhang Z (2004) Crystal structure of quinone reductase 2 in complex with resveratrol. *Biochemistry* **43:**11417–11426 doi: 10.1021/bi049162o.

Cassagnes LE, Perio P, Ferry G, Moulharat N, Antoine M, Gayon R, Boutin JA, Nepveu F, and Reybier K (2015) In cellulo monitoring of quinone reductase activity and reactive oxygen species production during the redox cycling of 1,2 and 1,4 quinones. *Free Radic. Biol. Med.* **89:**126–134 doi: 10.1016/j.freeradbiomed.2015.07.150.

Cassagnes LE, Rakotoarivelo N, Sirigu S, Perio P, Najahi E, Chavas LM, Thompson A, Gayon R, Ferry G, Boutin JA, Valentin A, Reybier K, and Nepveu F (2017) Role of Quinone Reductase 2 in the Antimalarial Properties of Indolone-Type Derivatives. *Molecules.* **22** doi: 10.3390/molecules22020210.

Cechelli R, Dehouck B, Descamps L, Fenart L, Buee-Scherrer V, Duhem C, Lundquist S, Rentfel L, Torpier G, and Dehouck MP (1999) In vitro model for evaluating drug transport across the blood-brain-barrier. *Adv. Drug Deliv. Rev.* **36:**165–178.

Chen D, Li X, Liu X, Liu X, Jiang X, Du J, Wang Q, Liang Y, and Ma W (2017) NQO2 inhibition relieves reactive oxygen species effects on mouse oocyte meiotic maturation and embryo development. *Biol Reprod* **97:**598–611 doi: 10.1093/biolre/iox098.

Conover TE and Ernster L (1960) Mitochondrial oxidation of extra-mitochondrial TPNH1 mediated by purified DT diaphorase. *Biochem Biophys Res Commun* **2:**26–30.

D'Amelio M, Puglisi-Allegra S, and Mercuri N (2018) The role of dopaminergic midbrain in Alzheimer's disease: Translating basic science into clinical practice. *Pharmacological Research* **130:**414–419 doi: 10.1016/j.phrs.2018.01.016.

Dagda RK, Das Banerjee T, and Janda E (2013) How Parkinsonian toxins dysregulate the autophagy machinery. *Int J Mol Sci* **14:**22163–22189 doi: 10.3390/ijms141122163.

den Braver-Sewradj SP, den Braver MW, Toorneman RM, van Leeuwen S, Zhang Y, Dekker SJ, Vermeulen NPE, Commandeur JNM, and Vos JC (2017) Reduction and scavenging of chemically reactive drug metabolites by NAD(P)H: Quinone oxidoreductase 1 and NRH:quinone oxidoreductase 2 and variability in hepatic concentrations. *Chem Res Toxicol* doi: 10.1021/acs.chemrestox.7b00289.

Duncan JS, Gyenis L, Lenehan J, Bretner M, Graves LM, Haystead TA, and Litchfield DW (2008) An unbiased evaluation of CK2 inhibitors by chemoproteomics: Characterization of inhibitor effects on CK2 and identification of novel inhibitor targets. *Mol Cell Proteomics* **7:**1077–1088 doi: 10.1074/mcp.M700559-MCP200.

Duncan MJ, Takahashi JS, and Dubocovich ML (1988) 2-[125I]iodomelatonin binding sites in hamster brain membranes: Pharmacological characteristics and regional distribution. *Endocrinology* **122:**1825–1833 doi: 10.1210/endo-122-5-1825.

Ennaceur A and Delacour J (1988) A new one-trial test for neurobiological studies of memory in rats. 1: Behavioral data. *Behav Brain Res* **31:**47–59.

Ernster L, Danielson L, and LJUNGGREN M (1962) DT diaphorase. I. Purification from the soluble fraction of rat-liver cytoplasm, and properties. *Biochim. Biophys. Acta* **58:**171–188.

Ferry G, Hecht S, Berger S, Moulharat N, Coge F, Guillaumet G, Leclerc V, Yous S, Delagrange P, and Boutin JA (2010) Old and new inhibitors of quinone reductase 2. *Chem. Biol. Interact.* **186:**103–109 doi: 10.1016/j.cbi.2010.04.006.

Gerard CJJ, Ferry G, Vuillard LM, Boutin JA, Ferte N, Grossier R, Candoni N, and Veesler S (2018) A Chemical Library to Screen Protein and Protein–Ligand Crystallization Using a Versatile Microfluidic Platform. *Crystal Growth & Design* doi: 10.1021/acs.cgd.8b00572.

Groß CJ, Mishra R, Schneider KS, Médard G, Wettmarshausen J, Dittlein DC, Shi H, Gorka O, Koenig P-A, Fromm S, Magnani G, Ćiković T, Hartjes L, Smollich J, Robertson AAB, Cooper MA, Schmidt-Supprian M, Schuster M, Schroder K, Broz P, Traidl-Hoffmann C, Beutler B, Kuster B, Ruland J, Schneider S, Perocchi F, and Groß O (2016) K + Efflux-Independent NLRP3 Inflammasome Activation by Small Molecules Targeting Mitochondria. *Immunity* **45:**761–773 doi: 10.1016/j.immuni.2016.08.010.

Guerreiro S, Toulorge D, Hirsch E, Marien M, Sokoloff P, and Michel PP (2008) Paraxanthine, the primary metabolite of caffeine, provides protection against dopaminergic cell death via stimulation of ryanodine receptor channels. *Mol. Pharmacol.* **74:**980–989 doi: 10.1124/mol.108.048207.

Harada S, Fujii C, Hayashi A, and Ohkoshi N (2001) An Association between Idiopathic Parkinson's Disease and Polymorphisms of Phase II Detoxification Enzymes: Glutathione S-Transferase M1 and Quinone Oxidoreductase 1 and 2. *Biochem Biophys Res Commun* **288:**887–892 doi: 10.1006/bbrc.2001.5868.

Janda E, Isidoro C, Carresi C, and Mollace V (2012) Defective autophagy in Parkinson's disease: Role of oxidative stress. *Mol Neurobiol* **46:**639–661 doi: 10.1007/s12035-012-8318-1.

Janda E, Lascala A, Carresi C, Parafati M, Aprigliano S, Russo V, Savoia C, Ziviani E, Musolino V, Morani F, Isidoro C, and Mollace V (2015) Parkinsonian toxin-induced oxidative stress inhibits basal autophagy in astrocytes via NQO2/quinone oxidoreductase 2: Implications for neuroprotection. *Autophagy.* **11:**1063–1080 doi: 10.1080/15548627.2015.1058683.

Janda E, Parafati M, Aprigliano S, Carresi C, Visalli V, Sacco I, Ventrice D, Mega T, Vadala N, Rinaldi S, Musolino V, Palma E, Gratteri S, Rotiroti D, and Mollace V (2013) The antidote effect of quinone oxidoreductase 2 inhibitor against paraquat-induced toxicity in vitro and in vivo. *Br. J Pharmacol.* **168:**46–59 doi: 10.1111/j.1476-5381.2012.01870.x.

Jiang Y, Liu J, Chen D, Yan L, and Zheng W (2017) Sirtuin Inhibition: Strategies, Inhibitors, and Therapeutic Potential. *Trends Pharmacol. Sci.* **38:**459–472 doi: 10.1016/j.tips.2017.01.009.

Kappus H and Sies H (1981) Toxic drug effects associated with oxygen metabolism: Redox cycling and lipid peroxidation. *Experientia* **37:**1233–1241.

Knox RJ, Burke PJ, Chen S, and Kerr DJ (2003) CB 1954: From the Walker tumor to NQO2 and VDEPT. *Curr. Pharm. Des* **9:**2091–2104.

Kuribayashi F, Tsuruta S, Yamazaki T, Nunoi H, Imajoh-Ohmi S, Kanegasaki S, and Nakamura M (2008) Cell adhesion markedly increases lucigenin-enhanced chemiluminescence of the phagocyte NADPH oxidase. *Genes Cells* **13:**1249–1256 doi: 10.1111/j.1365-2443.2008.01241.x.

Kuznetsov AV, Veksler V, Gellerich FN, Saks V, Margreiter R, and Kunz WS (2008) Analysis of mitochondrial function in situ in permeabilized muscle fibers, tissues and cells. *Nat. Protoc.* **3:**965–976 doi: 10.1038/nprot.2008.61.

Kwiek JJ, Haystead TA, and Rudolph J (2004) Kinetic mechanism of quinone oxidoreductase 2 and its inhibition by the antimalarial quinolines. *Biochemistry* **43:**4538–4547 doi: 10.1021/bi035923w.

Lascala A, Martino C, Parafati M, Salerno R, Oliverio M, Pellegrino D, Mollace V, and Janda E (2018) Analysis of proautophagic activities of Citrus flavonoids in liver cells reveals the superiority of a natural polyphenol mixture over pure flavones. *The Journal of Nutritional Biochemistry* **58:**119–130 doi: 10.1016/j.jnutbio.2018.04.005.

Lavrado J, Paulo A, Gut J, Rosenthal PJ, and Moreira R (2008) Cryptolepine analogues containing basic aminoalkyl side-chains at C-11: Synthesis, antiplasmodial activity, and cytotoxicity. *Bioorganic & Medicinal Chemistry Letters* **18:**1378–1381 doi: 10.1016/j.bmcl.2008.01.015.

Leung KK and Shilton BH (2013) Chloroquine binding reveals flavin redox switch function of quinone reductase 2. *J Biol. Chem.* **288:**11242–11251 doi: 10.1074/jbc.M113.457002.

Leung KK and Shilton BH (2015) Quinone reductase 2 is an adventitious target of protein kinase CK2 inhibitors TBBz (TBI) and DMAT. *Biochemistry* **54:**47–59 doi: 10.1021/bi500959t.

Liao S, Dulaney J, and Willaims-Ashman HG (1962) Purification and properties of a flavoprotein catalyzing the oxidation of reduced ribosyl nicotinamide. *J Biol. Chem.* **237:**2981–2987.

Liao S and Williams-Ashman HG (1961) Enzymatic oxidation of some non-phosphorylated derivatives of dihydronicotinamide. *Biochem. Biophys. Res Commun.* **4:**208–213.

Mailliet F, Ferry G, Vella F, Thiam K, Delagrange P, and Boutin JA (2004) Organs from mice deleted for NRH:quinone oxidoreductase 2 are deprived of the melatonin binding site MT3. *FEBS Lett.* **578:**116–120 doi: 10.1016/j.febslet.2004.10.083.

McNab F, Varrone A, Farde L, Jucaite A, Bystritsky P, Forssberg H, and Klingberg T (2009) Changes in Cortical Dopamine D1 Receptor Binding Associated with Cognitive Training. *Science* **323:**800–802 doi: 10.1126/science.1166102.

Michaelis S, Marais A, Schrey AK, Graebner OY, Schaudt C, Sefkow M, Kroll F, Dreger M, Glinski M, Koester H, Metternich R, and Fischer JJ (2012) Dabigatran and dabigatran ethyl ester: Potent inhibitors of ribosyldihydronicotinamide dehydrogenase (NQO2). *J. Med. Chem.* **55:**3934–3944 doi: 10.1021/jm3001339.

Millan MJ, La Mannoury Cour C, Chanrion B, Dupuis DS, Di Cara B, Audinot V, Cussac D, Newman-Tancredi A, Kamal M, Boutin JA, Jockers R, Marin P, Bockaert J, Muller O, Dekeyne A, and Lavielle G (2012) S32212, a Novel Serotonin Type 2C Receptor Inverse Agonist/ 2-Adrenoceptor Antagonist and Potential Antidepressant: I. A Mechanistic Characterization. *Journal of Pharmacology and Experimental Therapeutics* **340:**750–764 doi: 10.1124/jpet.111.187468.

Nishiyama T, Izawa T, Usami M, Ohnuma T, Ogura K, and Hiratsuka A (2010) Cooperation of NAD(P)H:quinone oxidoreductase 1 and UDP-glucuronosyltransferases reduces menadione cytotoxicity in HEK293 cells. *Biochem. Biophys. Res Commun.* **394:**459–463 doi: 10.1016/j.bbrc.2009.12.113.

Nobili A, Latagliata EC, Viscomi MT, Cavallucci V, Cutuli D, Giacovazzo G, Krashia P, Rizzo FR, Marino R, Federici M, Bartolo P de, Aversa D, Dell'Acqua MC, Cordella A, Sancandi M, Keller F, Petrosini L, Puglisi-Allegra S, Mercuri NB, Coccurello R, Berretta N, and D'Amelio M (2017) Dopamine neuronal loss contributes to memory and reward dysfunction in a model of Alzheimer's disease. *Nat Comms* **8:**14727 doi: 10.1038/ncomms14727.

Nosjean O, Ferro M, Coge F, Beauverger P, Henlin JM, Lefoulon F, Fauchere JL, Delagrange P, Canet E, and Boutin JA (2000) Identification of the melatonin-binding site MT3 as the quinone reductase 2. *J Biol. Chem.* **275:**31311–31317 doi: 10.1074/jbc.M005141200.

Nosjean O, Nicolas JP, Klupsch F, Delagrange P, Canet E, and Boutin JA (2001) Comparative pharmacological studies of melatonin receptors: MT1, MT2 and MT3/QR2. Tissue distribution of MT3/QR2. *Biochem. Pharmacol.* **61:**1369–1379.

Nutter LM, Ngo EO, Fisher GR, and Gutierrez PL (1992) DNA strand scission and free radical production in menadione-treated cells. Correlation with cytotoxicity and role of NADPH quinone acceptor oxidoreductase. *J Biol. Chem.* **267:**2474–2479.

Onyeibor O, Croft SL, Dodson HI, Feiz-Haddad M, Kendrick H, Millington NJ, Parapini S, Phillips RM, Seville S, Shnyder SD, Taramelli D, and Wright CW (2005) Synthesis of Some Cryptolepine Analogues, Assessment of Their Antimalarial and Cytotoxic Activities, and Consideration of Their Antimalarial Mode of Action. *J. Med. Chem.* **48:**2701–2709 doi: 10.1021/jm040893w.

Paul P, Lahaye C, Delagrange P, Nicolas JP, Canet E, and Boutin JA (1999) Characterization of 2-[125I]iodomelatonin binding sites in Syrian hamster peripheral organs. *J Pharmacol. Exp. Ther.* **290:**334–340.

Pegan SD, Sturdy M, Ferry G, Delagrange P, Boutin JA, and Mesecar AD (2011) X-ray structural studies of quinone reductase 2 nanomolar range inhibitors. *Protein Sci.* **20:**1182–1195 doi: 10.1002/pro.647.

Perry CG, Kane DA, Lanza IR, and Neufer PD (2013) Methods for assessing mitochondrial function in diabetes. *Diabetes* **62:**1041–1053 doi: 10.2337/db12-1219.

Perry CG, Kane DA, Lin CT, Kozy R, Cathey BL, Lark DS, Kane CL, Brophy PM, Gavin TP, Anderson EJ, and Neufer PD (2011) Inhibiting myosin-ATPase reveals a dynamic range of mitochondrial respiratory control in skeletal muscle. *Biochem. J* **437:**215–222 doi: 10.1042/BJ20110366.

Pesta D and Gnaiger E (2012) High-resolution respirometry: OXPHOS protocols for human cells and permeabilized fibers from small biopsies of human muscle. *Methods Mol. Biol.* **810:**25–58 doi: 10.1007/978-1-61779-382-0_3.

Polster BM, Nicholls DG, Ge SX, and Roelofs BA (2014) Use of potentiometric fluorophores in the measurement of mitochondrial reactive oxygen species. *Meth Enzymol* **547:**225–250 doi: 10.1016/B978-0-12-801415-8.00013-8.

Rappaport AN, Jacob E, Sharma V, Inberg S, Elkobi A, Ounallah-Saad H, Pasmanik-Chor M, Edry E, and Rosenblum K (2015) Expression of Quinone Reductase-2 in the Cortex Is a Muscarinic Acetylcholine Receptor-Dependent Memory Consolidation Constraint. *J. Neurosci.* **35:**15568–15581 doi: 10.1523/JNEUROSCI.1170-15.2015.

Reddy PVN, Jensen KC, Mesecar AD, Fanwick PE, and Cushman M (2011) Design, Synthesis, and Biological Evaluation of Potent Quinoline and Pyrroloquinoline Ammosamide Analogues as Inhibitors of Quinone Reductase 2. *J. Med. Chem.* **55:**367–377 doi: 10.1021/jm201251c.

Reybier K, Perio P, Ferry G, Bouajila J, Delagrange P, Boutin JA, and Nepveu F (2011) Insights into the redox cycle of human quinone reductase 2. *Free Radic. Res* **45:**1184–1195 doi: 10.3109/10715762.2011.605788.

Rix U, Hantschel O, Durnberger G, Remsing Rix LL, Planyavsky M, Fernbach NV, Kaupe I, Bennett KL, Valent P, Colinge J, Kocher T, and Superti-Furga G (2007) Chemical proteomic profiles of the BCR-ABL inhibitors imatinib, nilotinib, and dasatinib reveal novel kinase and nonkinase targets. *Blood* **110:**4055–4063 doi: 10.1182/blood-2007-07-102061.

Rossato JI, Bevilaqua LRM, Izquierdo I, Medina JH, and Cammarota M (2009) Dopamine Controls Persistence of Long-Term Memory Storage. *Science* **325:**1017–1020 doi: 10.1126/science.1172545.

Salthun-Lassalle B, Hirsch EC, Wolfart J, Ruberg M, and Michel PP (2004) Rescue of mesencephalic dopaminergic neurons in culture by low-level stimulation of voltage-gated sodium channels. *J. Neurosci.* **24:**5922–5930 doi: 10.1523/JNEUROSCI.5668-03.2004.

Sasaki S, Yamada S, Iwamura M, and Kobayashi Y (2013) Specific detection of intramitochondrial superoxide produced by either cell activation or apoptosis by employing a newly developed cell-permeative lucigenin derivative, 10,10'-dimethyl-9,9'-biacridinium bis(monomethyl terephthalate). *Free Radic. Biol. Med.* **65:**1005–1011 doi: 10.1016/j.freeradbiomed.2013.08.175.

Scott KA, Barnes J, Whitehead RC, Stratford IJ, and Nolan KA (2011) Inhibitors of NQO1: Identification of compounds more potent than dicoumarol without associated off-target effects. *Biochem Pharmacol* **81:**355–363 doi: 10.1016/j.bcp.2010.10.011.

Sorce S, Stocker R, Seredenina T, Holmdahl R, Aguzzi A, Chio A, Depaulis A, Heitz F, Olofsson P, Olsson T, Duveau V, Sanoudou D, Skosgater S, Vlahou A, Wasquel D, Krause K-H, and Jaquet V (2017) NADPH oxidases as drug targets and biomarkers in neurodegenerative diseases: What is the evidence? *Free Radic. Biol. Med.* **112:**387–396 doi: 10.1016/j.freeradbiomed.2017.08.006.

Teixeira G, Szyndralewiez C, Molango S, Carnesecchi S, Heitz F, Wiesel P, and Wood JM (2017) Therapeutic potential of NADPH oxidase ¼ inhibitors. *Br. J Pharmacol.* **174:**1647–1669 doi: 10.1111/bph.13532.

Toulorge D, Guerreiro S, Hild A, Maskos U, Hirsch EC, and Michel PP (2011) Neuroprotection of midbrain dopamine neurons by nicotine is gated by cytoplasmic Ca2+. *FASEB J* **25:**2563–2573 doi: 10.1096/fj.11-182824.

Troadec J-D, Marien M, Darios F, Hartmann A, Ruberg M, Colpaert F, and Michel PP (2001) Noradrenaline provides long-term protection to dopaminergic neurons by reducing oxidative stress. *J Neurochem.* **79:**200–210 doi: 10.1046/j.1471-4159.2001.00556.x.

Whittell LR, Batty KT, Wong RPM, Bolitho EM, Fox SA, Davis TME, and Murray PE (2011) Synthesis and antimalarial evaluation of novel isocryptolepine derivatives. *Bioorganic & Medicinal Chemistry* **19:**7519–7525 doi: 10.1016/j.bmc.2011.10.037.

Wosilait WD and Nason A (1954) Pyridine nucleotide-quinone reductase. I. Purification and properties of the enzyme from pea seeds. *J Biol. Chem.* **206:**255–270.

Wu K, Knox R, Sun XZ, Joseph P, Jaiswal AK, Zhang D, Deng PS, and Chen S (1997) Catalytic properties of NAD(P)H:quinone oxidoreductase-2 (NQO2), a dihydronicotinamide riboside dependent oxidoreductase. *Arch. Biochem. Biophys.* **347:**221–228 doi: 10.1006/abbi.1997.0344.

Zhao Q, Yang XL, Holtzclaw WD, and Talalay P (1997) Unexpected genetic and structural relationships of a long-forgotten flavoenzyme to NAD(P)H:quinone reductase (DT-diaphorase). *Proc. Natl. Acad. Sci. U. S. A* **94:**1669–1674.

Table 1: Summary of the IC_{50} obtained in different laboratories and conditions with S29434

Enzyme	Co-substrate	Substrate	Signal	IC_{50} (nM)	References
h QR2 expressed in *E. coli*	BNAH (100 µM)	Menadione	Abs* 350 nm	20	Unpublished
h QR2 expressed in *E. coli*	NRH (100 µM)	Menadione	Abs* 340 nm	5	Unpublished
h QR2 expressed in CHO	BNAH (100 µM)	Menadione	Fluo** BNAH	14	(Pegan et al., 2011)
h QR2 expressed in *E. coli*	NMeH (100 µM)	Menadione	Abs* 360 nm	2.4	(Pegan et al., 2011)
h QR2 expressed in *E. coli*	NMeH (100 µM)	Formosan	Abs*** 612 nm	2.4	(Pegan et al., 2011)
h QR2 expressed in insect cells	BNAH (100 µM)	Menadione	Fluo** BNAH	7	(Ferry et al., 2010)
h QR2 expressed in insect cells	NRH (100 µM)	Menadione	Fluo** NRH	0.7	(Ferry et al., 2010)

Notes: *Abs: absorbance assay; ** Fluo: fluorimetric assay; *** Abs of MTT.

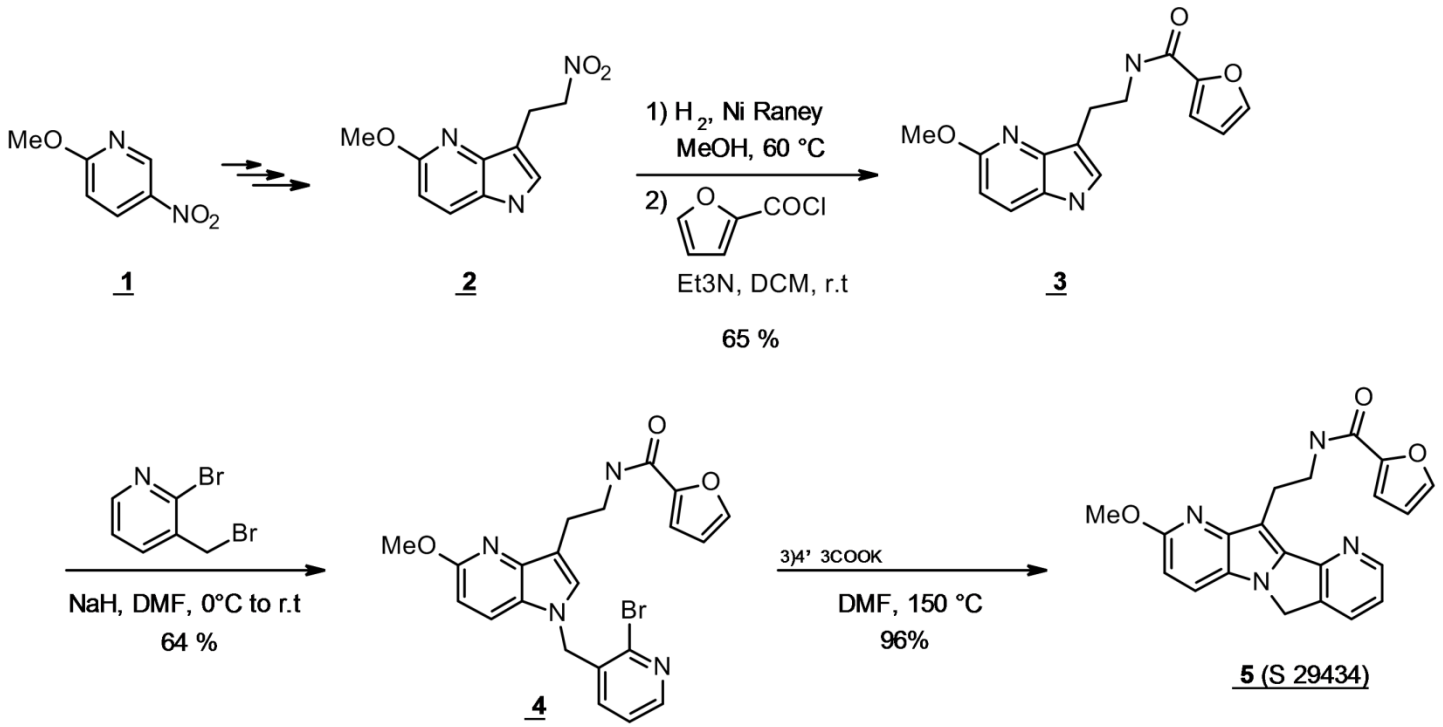
MeO
N
NO2
1
2
1) H2, Ni Raney
MeOH, 60 °C
2)
COCl
Et3N, DCM, r.t
65 %
3
NaH, DMF, 0°C to r.t
64 %
Br
4
3)4' 3COOK
DMF, 150 °C
96%
5 (S 29434)

Figure 1

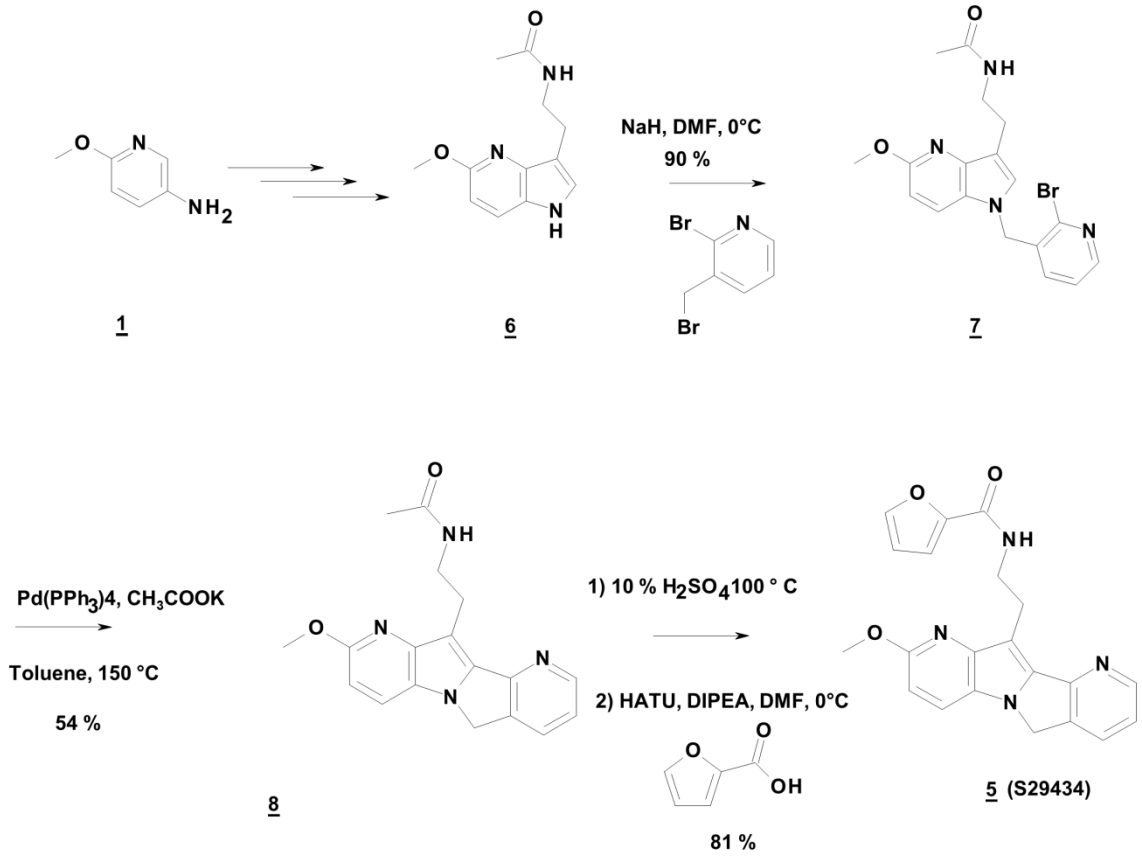
NaH, DMF, 0°C
90 %
Pd(PPh3)4, CH3COOK
Toluene, 150 °C
54 %
1) 10 % H2SO4 100 ° C
2) HATU, DIPEA, DMF, 0°C
81 %
1
6
7
8
5 (S29434)

Figure 2

A

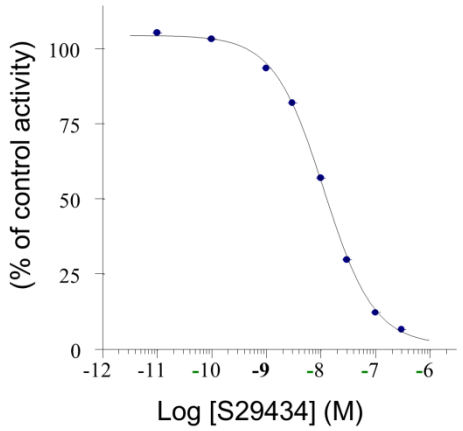
(% of control activity)
100
75
50
25
0
-12
-11
-10
-9
-8
-7
-6
Log [S29434] (M)

B

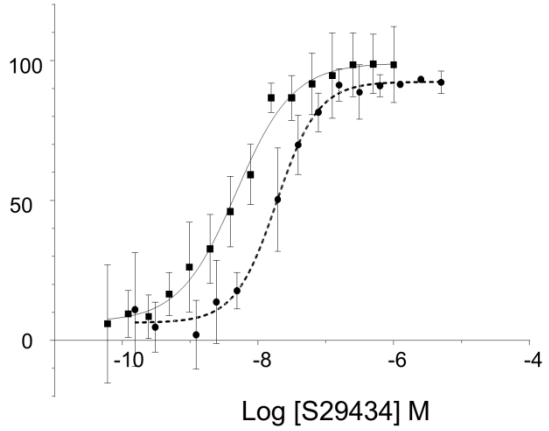
100
50
0
-10
-8
-6
-4
Log [S29434] M

Figure 3

QR1

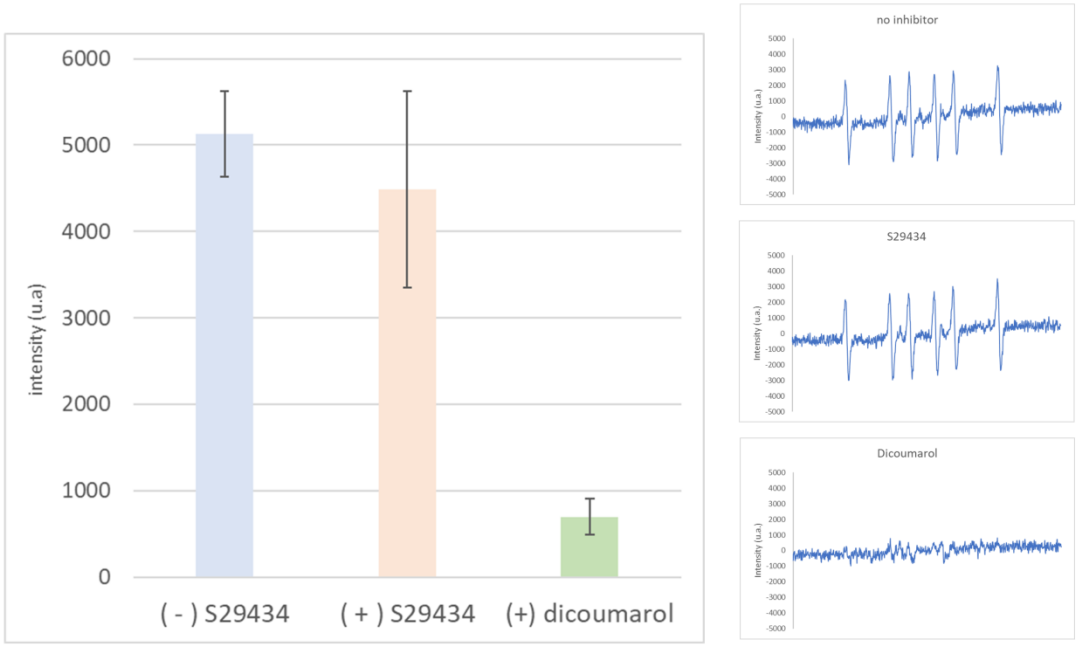

Figure now 4

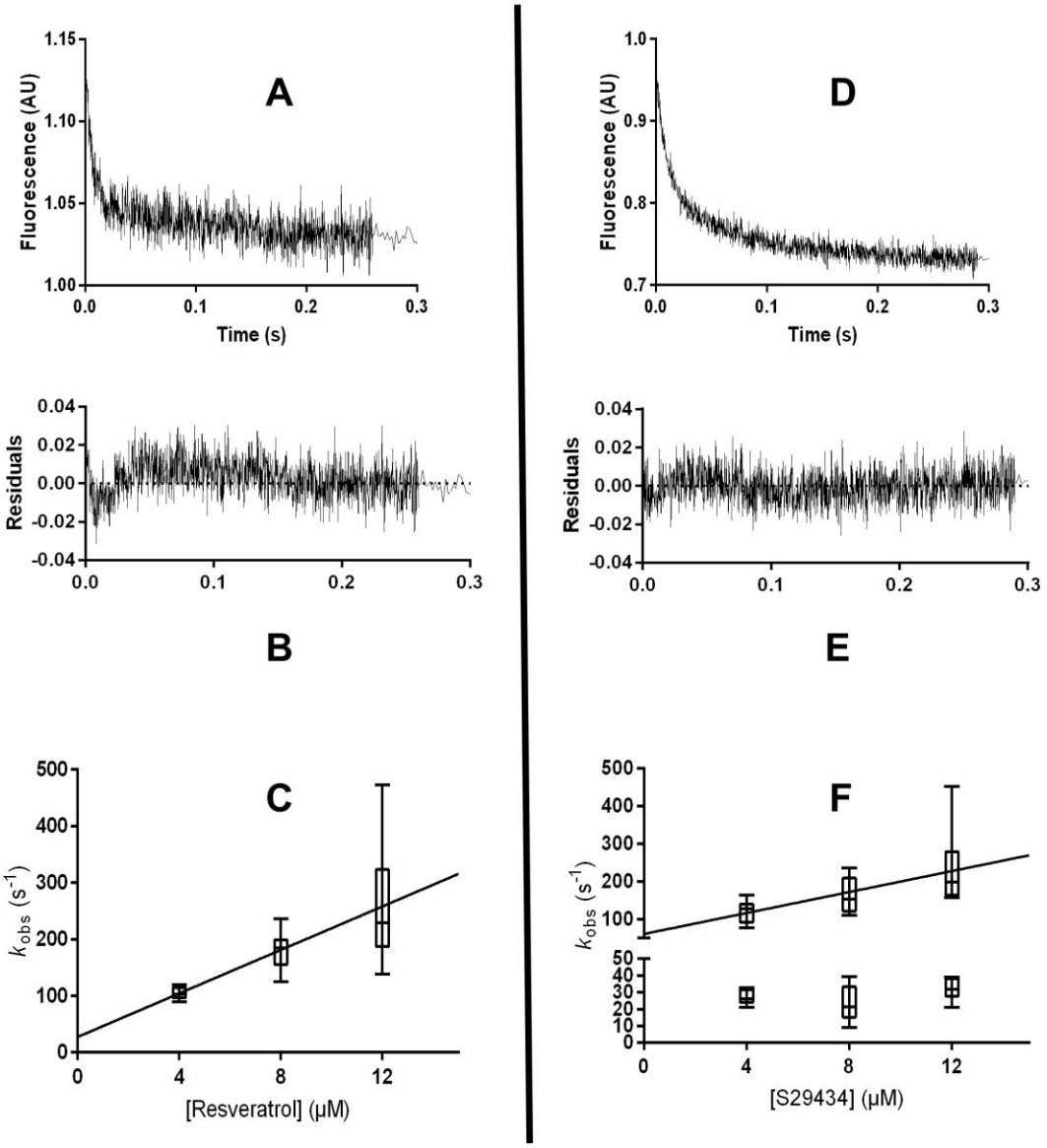
A
Fluorescence (AU)
Time (s)
Residuals
B
C
k_{obs} (s^{-1})
[Resveratrol] (μM)
D
Fluorescence (AU)
Time (s)
Residuals
E
F
k_{obs} (s^{-1})
[S29434] (μM)

Figure 5

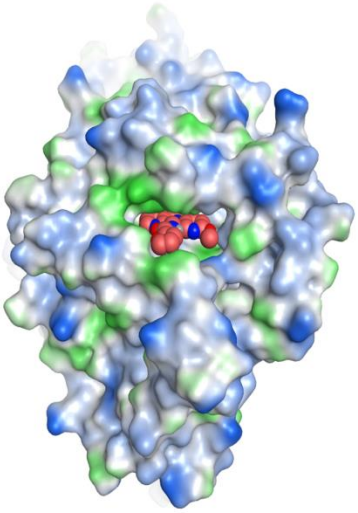

A

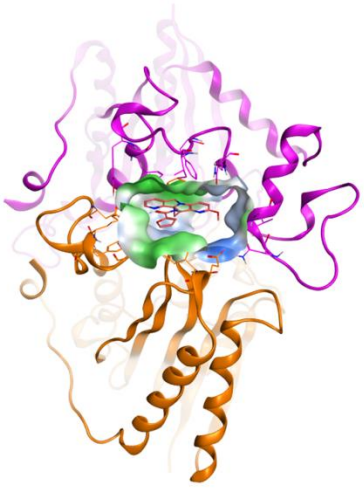

B

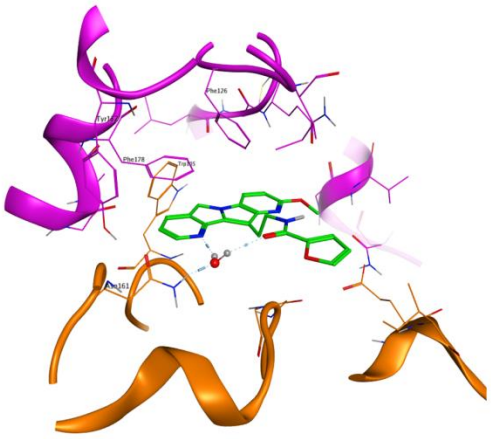

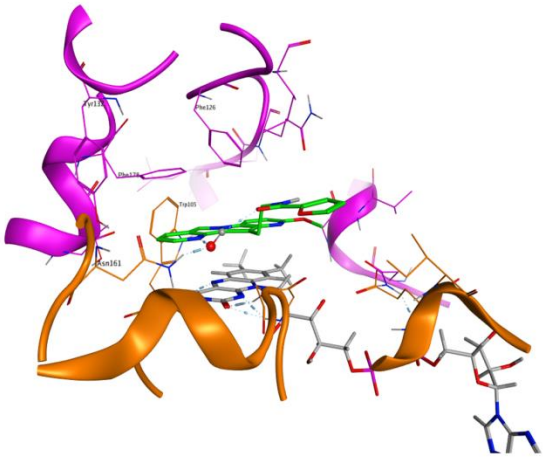

C

Figure 6

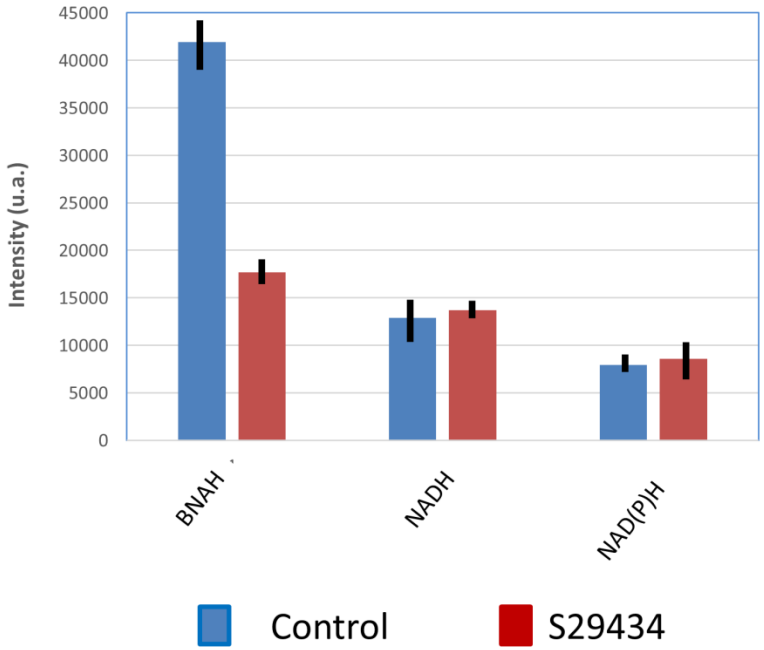
45000
40000
35000
30000
25000
20000
15000
10000
5000
0
Intensity (u.a.)
BNAH
NADH
NAD(P)H
Control
S29434

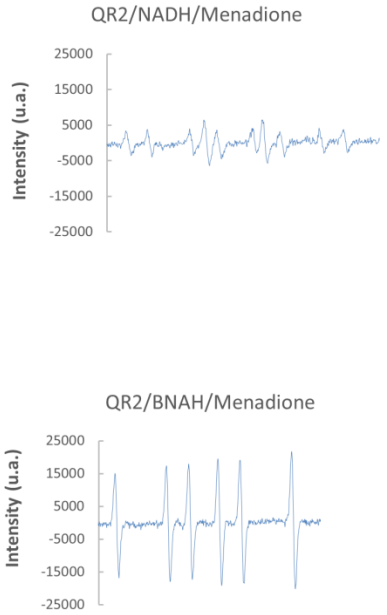
QR2/NADH/Menadione
Intensity (u.a.)
25000
15000
5000
-5000
-15000
-25000
QR2/BNAH/Menadione
Intensity (u.a.)
25000
15000
5000
-5000
-15000
-25000

Figure 7

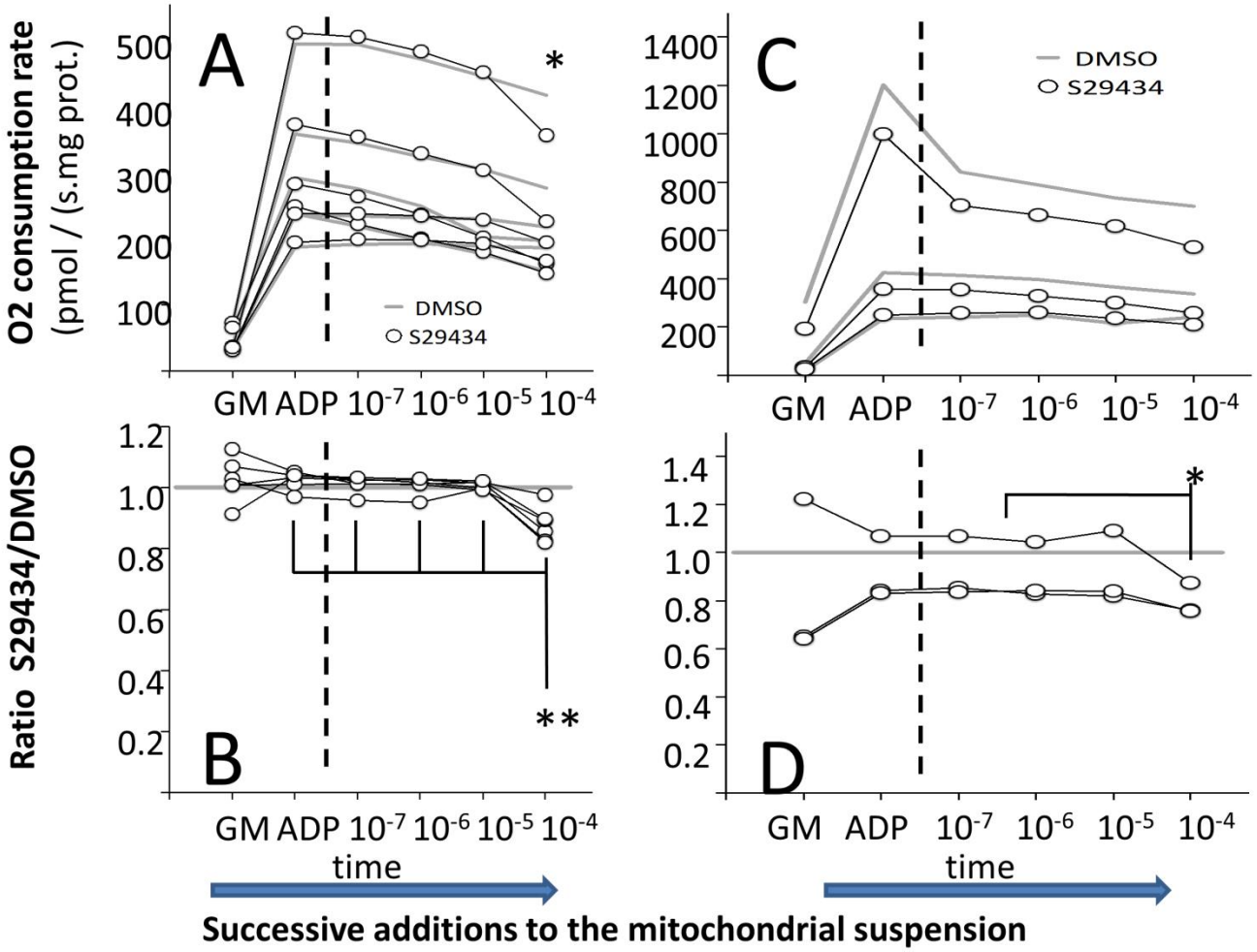
O2 consumption rate
(pmol / (s.mg prot.)
A
B
C
D
DMSO
S29434
Ratio S29434/DMSO
GM ADP 10-7 10-6 10-5 10-4
time
Successive additions to the mitochondrial suspension

Figure 8

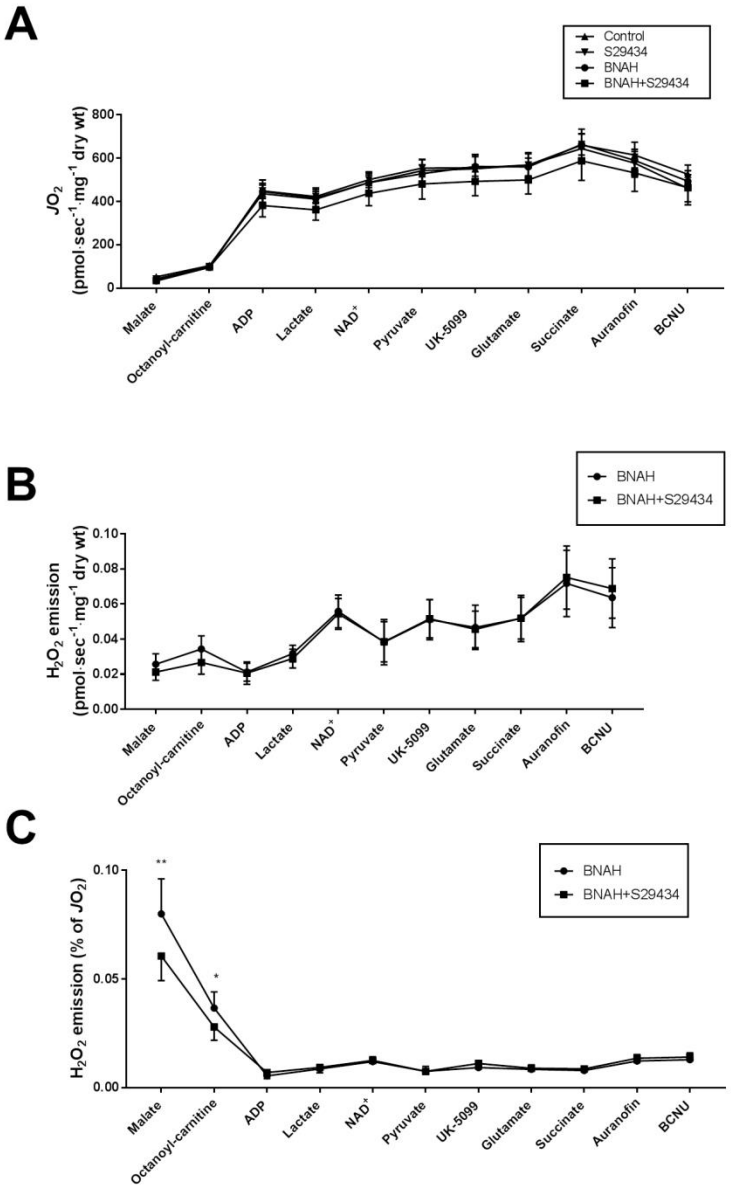
A
Control
S29434
BNAH
BNAH+S29434
JO2 (pmol·sec-1·mg-1 dry wt)
0
200
400
600
800
Malate
Octanoyl-carnitine
ADP
Lactate
NAD+
Pyruvate
UK-5099
Glutamate
Succinate
Auranofin
BCNU
B
BNAH
BNAH+S29434
H2O2 emission (pmol·sec-1·mg-1 dry wt)
0.00
0.02
0.04
0.06
0.08
0.10
Malate
Octanoyl-carnitine
ADP
Lactate
NAD+
Pyruvate
UK-5099
Glutamate
Succinate
Auranofin
BCNU
C
BNAH
BNAH+S29434
H2O2 emission (% of JO2)
0.00
0.05
0.10
**
*
Malate
Octanoyl-carnitine
ADP
Lactate
NAD+
Pyruvate
UK-5099
Glutamate
Succinate
Auranofin
BCNU

Figure 9

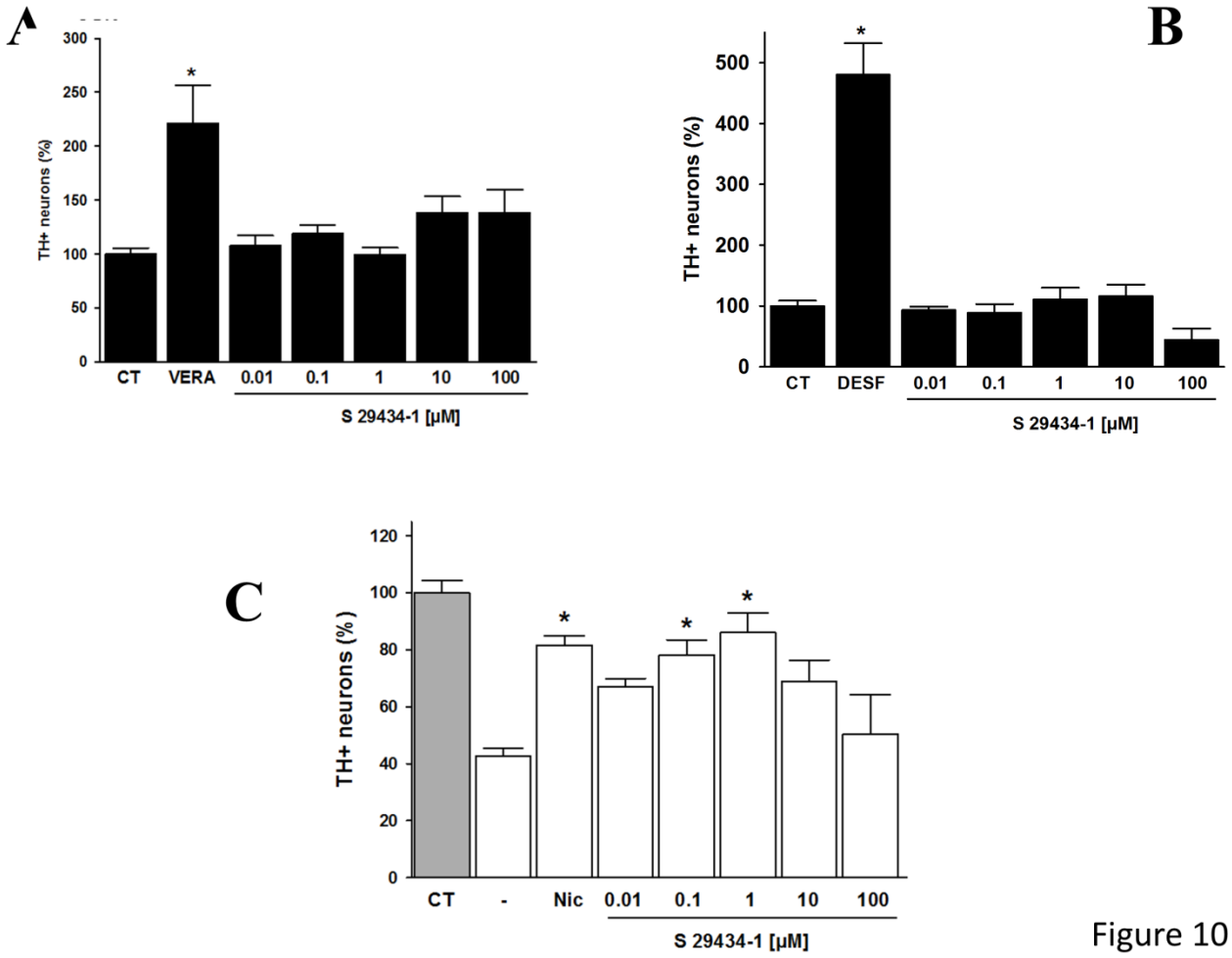
A
TH+ neurons (%)
300
250
200
150
100
50
0
*
CT
VERA
0.01
0.1
1
10
100
S 29434-1 [µM]
B
TH+ neurons (%)
500
400
300
200
100
0
*
CT
DESF
0.01
0.1
1
10
100
S 29434-1 [µM]
C
TH+ neurons (%)
120
100
80
60
40
20
0
*
*
*
CT
-
Nic
0.01
0.1
1
10
100
S 29434-1 [µM]

Figure 10

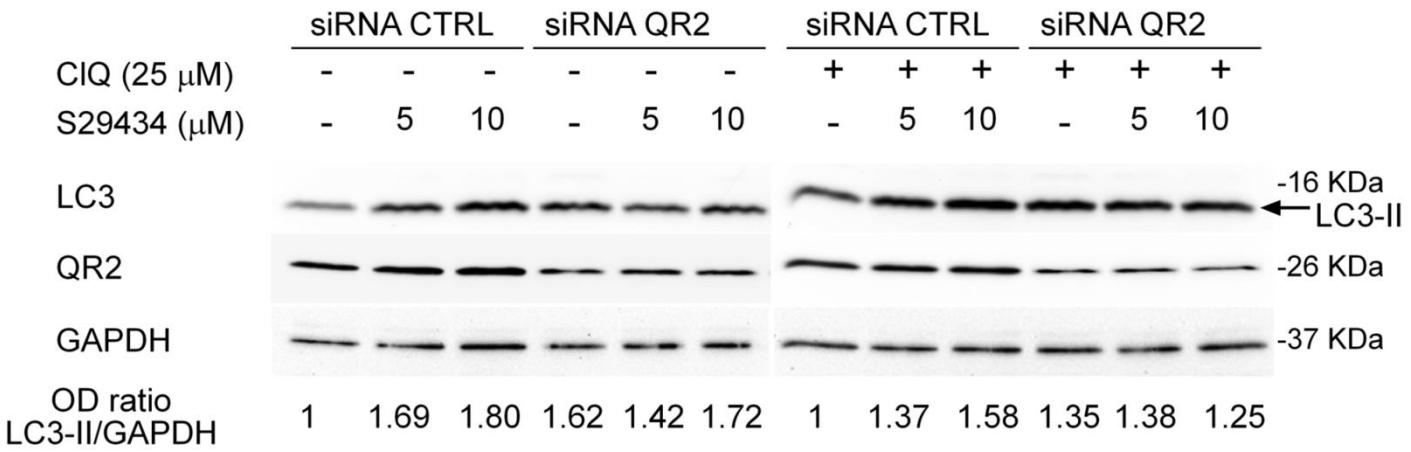
siRNA CTRL
siRNA QR2
siRNA CTRL
siRNA QR2
ClQ (25 μM) - - - - - - + + + + + +
S29434 (μM) - 5 10 - 5 10 - 5 10 - 5 10
LC3
-16 KDa
LC3-II
QR2
-26 KDa
GAPDH
-37 KDa
OD ratio LC3-II/GAPDH
1 1.69 1.80 1.62 1.42 1.72 1 1.37 1.58 1.35 1.38 1.25

Fig. 11

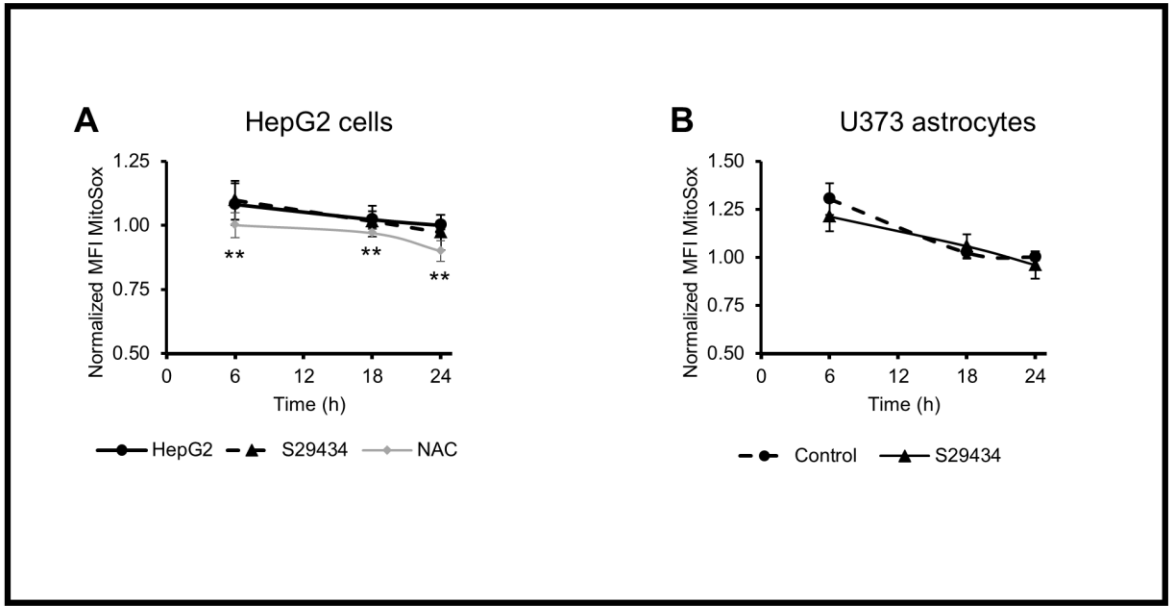
A
HepG2 cells
Normalized MFI MitoSox
1.25
1.00
0.75
0.50
0
6
12
18
24
Time (h)
**
**
**
HepG2
S29434
NAC
B
U373 astrocytes
Normalized MFI MitoSox
1.50
1.25
1.00
0.75
0.50
0
6
12
18
24
Time (h)
Control
S29434

Figure 12

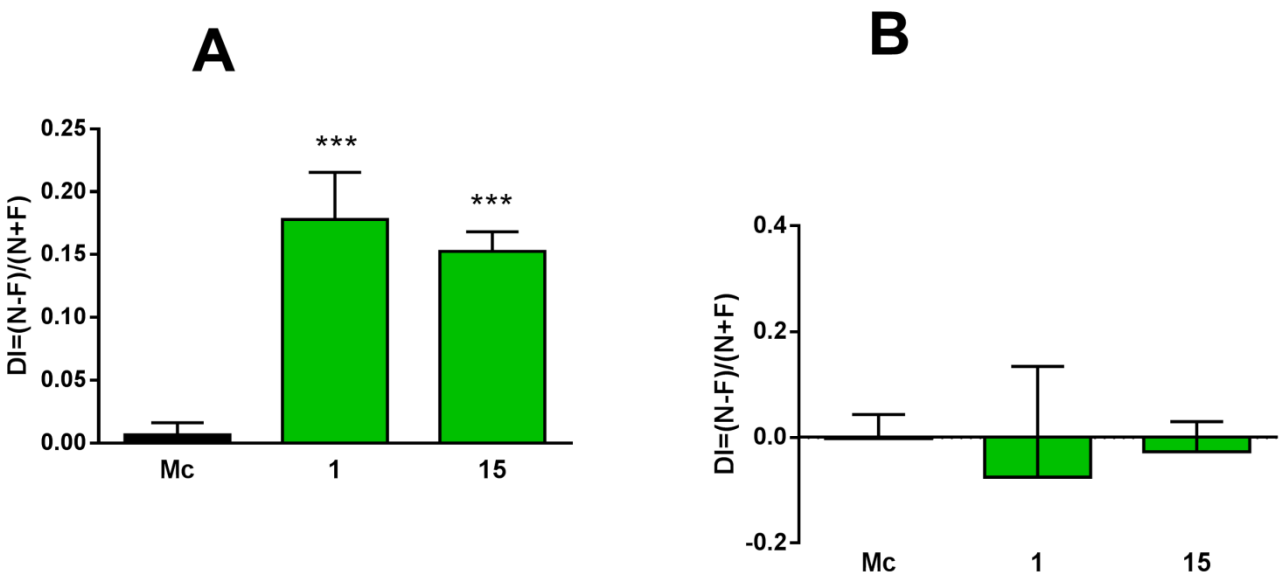
A
0.25
0.20
0.15
0.10
0.05
0.00
DI=(N-F)/(N+F)
***
***
Mc
1
15
B
0.4
0.2
0.0
-0.2
DI=(N-F)/(N+F)
Mc
1
15

Figure 13